Atmos. Meas. Tech. Discuss., 2, 2919–2982, 2009
www.atmos-meas-tech-discuss.net/2/2919/2009/

Atmospheric Measurement Techniques Discussions

This discussion paper is/has been under review for the journal Atmospheric Measurement Techniques (AMT). Please refer to the corresponding final paper in AMT if available.

Extending differential optical absorption spectroscopy for limb measurements in the UV

J. Puķīte[1], S. Kühl[1], T. Deutschmann[2], U. Platt[2], and T. Wagner[1]

[1]Max Planck Institute for Chemistry, J. J. Becher Weg 27, 55128 Mainz, Germany
[2]Institute of Environmental Physics, University of Heidelberg, Im Neuenheimer Feld 229, 69120 Heidelberg, Germany

Received: 24 September 2009 – Accepted: 4 November 2009
– Published: 18 November 2009

Correspondence to: J. Puķīte (janis.pukite@mpch-mainz.mpg.de)

Published by Copernicus Publications on behalf of the European Geosciences Union.

Abstract

Methods of UV/VIS absorption spectroscopy to determine the constituents in the Earth's atmosphere from measurements of scattered light are often based on the Beer-Lambert law, like e.g. Differential Optical Absorption Spectroscopy (DOAS). Therefore they are strictly valid for weak absorptions and narrow wavelength intervals (strictly only for monochromatic radiation). For medium and strong absorption (e.g. along very long light-paths like in limb geometry) the relation between the optical depth and the concentration of an absorber is not linear anymore. As well, for large wavelength intervals the wavelength dependent differences in the travelled light-paths become important, especially in the UV, where the probability for scattering increases strongly with decreasing wavelength.

However, by taking into account these dependencies, the applicability of the DOAS method can be extended also to cases with medium to strong absorptions and for broader wavelength intervals.

Common approaches for this correction are the so called air mass factor modified (or extended) DOAS and the weighting function modified DOAS. These approaches take into account the wavelength dependency of the slant column densities (SCDs), but also require a-priori knowledge for the air mass factor or the weighting function calculation by radiative transfer modelling.

We describe an approach that considers the fitting results obtained from DOAS, the SCDs, as a function of wavelength and vertical optical depth and expands this function into a Taylor series of both quantities. The Taylor coefficients are then applied as additional fitting parameters in the DOAS analysis. Thus the variability of the SCD in the fit window is determined by the retrieval itself.

This new approach gives a description of the SCD that is as close to reality as desired (depending on the order of the Taylor expansion), and is independent from any assumptions or a-priori knowledge of the considered absorbers.

AMTD

2, 2919–2982, 2009

In case studies for simulated and measured spectra in the UV (332–357 nm), we demonstrate the improvement by this approach for the retrieval of vertical profiles of BrO from the SCIAMACHY limb observations. Compared to the standard DOAS approach, the results for BrO obtained from the simulated spectra are closer to the true profile, when applying the new method for the SCDs of ozone. Also for the measured spectra the agreement with validation measurements is improved significantly, especially for cases with strong ozone absorption.

While the focus of this article is on the improvement of the BrO profile retrieval from the SCIAMACHY limb measurements, the novel approach may be applied for a wide range of DOAS retrievals.

1 Introduction

Differential Optical Absorption Spectroscopy (DOAS) (Platt, 1994) is nowadays widely used to derive trace gas abundances in the atmosphere. Advancing former optical absorption techniques (Brewer et al., 1973; Noxon, 1975), DOAS has originally been invented and applied for ground based measurements of direct light (Perner et al., 1976; Platt et al., 1979; Platt and Perner, 1980, 1983). Later, the application was extended to observations of scattered light from ground, balloon, aircraft and satellite platforms (e.g. Platt and Stutz, 2008; Mount et al., 1987; Solomon et al., 1987; Wahner et al., 1990; Pfeilsticker and Platt, 1994; Burrows et al., 1999; Wagner et al., 2008). Compared to direct light measurements, where the light path is well defined, the observations for scattered light are usually characterized by complex viewing geometries, especially for observations at large SZA or for limb observations (i.e. at tangential view from satellites into the Earth's atmosphere). Therefore, the interpretation of the measurements often requires advanced radiative transfer modelling (RTM) and inversion algorithms.

For direct light observations using e.g. the sun or moon as light source, the detected integrated number density along the light path, the slant column density, SCD, is related

AMTD
2, 2919–2982, 2009

to the vertical column density, VCD (being the number density integrated along the altitude) by an enhancement factor (so called air mass factor, AMF) resulting only from the observation angle, i.e. can be calculated by simple trigonometry. For observations of scattered light however this enhancement factor is no more a pure geometric quantity but depends strongly on the individual path(s) that the light contributing to the measurement took in the atmosphere (e.g. Solomon et al., 1987; Perliski and Solomon, 1993).

This AMF depends on all factors that impact the light propagation in the atmosphere (like the Solar Zenith Angle, SZA, the air density, the abundance of absorbers like e.g. ozone, clouds, aerosols, albedo etc.) and therefore needs to be derived from RTM. In particular, due to the dependence of the propagation of light on scattering and absorption processes, the AMF is a function of wavelength and the absorption strength (Marquard et al., 2000). For the application of DOAS this means that the relation between the SCD and the VCD may vary considerably within the wavelength interval chosen for a DOAS fit (Platt et al., 1997).

While the wavelength dependency of the SCD can be neglected for many applications, it was found that it becomes important for cases with strong absorption (like e.g. absorption by ozone in the UV) and large SZA for satellite nadir and ground observations (Diebel et al., 1995; Richter, 1997). For limb geometry, where the atmosphere is observed in a tangential view, a correction for these effects is even more necessary due to the increased light paths.

An approach to correct for the wavelength dependency of the SCD in nadir and ground measurements is the so called AMF modified or extended DOAS (Diebel et al., 1995; Richter, 1997) which considers the product of the AMFs and the absorption cross-sections in the DOAS analysis instead of the cross-sections alone. Thus, wavelength independent VCDs are fitted directly.

However, of those factors determining the AMF for scattered light observations, only some are known before hand (like for example the observation geometry). Others like the (vertical) distribution of trace gases, clouds and aerosols in the atmosphere as well

AMTD
2, 2919–2982, 2009

as the air density (depending on pressure and temperature) are generally not known before the measurement. Therefore a-priori information is required to calculate the AMFs (and an iterative approach should be applied). Furthermore, large computational resources are required since the calculation of the AMFs needs to be performed for all wavelengths in the fit window.

Alternatively, the weighting function DOAS method (Buchwitz et al., 2000; Coldewey-Egbers et al., 2004, 2005; Frankenberg et al., 2005) was developed. It accounts for the wavelength modulation of the slant path by approximating the measured optical depth with a Taylor expansion around the reference intensity at a certain a-priori state plus a low order polynomial. The approach is performed for every wavelength and at a certain intensity, thus requiring both usage of a-priori information and calculation of intensity and weighting functions for every wavelength in the fit window as well.

In this article, we propose a method that takes into account the dependency of the SCDs from optical depth and also from wavelength already in the fitting procedure itself. Thus, wavelength dependent SCDs are determined by DOAS. The pre-calculation of AMFs or weighting functions and intensities is not required and the approach does not need a-priori input for the retrieval of SCDs. The method is based on the formulation of the AMFs (and consequently SCDs) as function of wavelength and optical depth of strong absorbers: a Taylor series expansion for AMFs or SCDs with respect to the wavelength and absorption by trace gases is performed.

The coefficients of this series are then co-fitted by the least squares approach like the absorption cross-sections in the standard DOAS. From the fitted coefficients, the functional relationship of the SCDs on wavelength and absorption can be determined and taken into account up to the precision of the order of the Taylor series expansion.

We study the capability and limitations of the method for the retrieval of vertical BrO profiles from ENVISAT/SCIAMACHY limb measurements in the near UV spectral region (332–357 nm). The method is applied for simulated and measured spectra for different fit windows. Also the effect of different ozone absorption strengths and geometries is investigated. By accounting for the variation of the ozone absorption in the

AMTD
2, 2919–2982, 2009

respective fit window, the BrO retrieval is improved as is demonstrated by comparing the retrieval results to the standard DOAS approach: for the simulated spectra the Taylor series approach for SCDs of ozone reduces the differences to the true profile of BrO significantly. Similarly, for spectra measured by SCIAMACHY, the new approach (which is applied on the two step method described in Puķīte et al., 2006; Kühl et al., 2008) results in a significantly better agreement with correlated balloon observations.

The article is structured as follows: in Sect. 2 we describe the standard DOAS approach, its limitations for strong absorptions and limb geometry and introduce the Taylor series approach to overcome this problem. Section 3 demonstrates the applicability of the approach to synthetic spectra, and Sect. 4 studies the sensitivity of the novel approach for different absorption strengths, geometries, fit windows and fit parameters. Section 5 shows the application of the approach to real measurements of SCIAMACHY and compares the result with correlated balloon measurements (Dorf et al., 2006). Last, Sect. 6 draws conclusions.

2 The method

2.1 Standard DOAS: principle and limitations for strong absorptions and scattered light

2.1.1 Standard DOAS

Differential Optical Absorption Spectroscopy (Platt, 1994) is an atmospheric spectroscopy method based on a modified Lambert-Beer law (extended to observations of scattered light), see e.g. Stutz and Platt (1996); Platt and Stutz (2008). To determine the SCDs S of the considered absorbing trace gases, DOAS utilizes their spectral features: the algorithm simultaneously fits the SCDs S_i of a number of k absorbers with

AMTD
2, 2919–2982, 2009

known absorption cross-sections σ_i to the difference of the logarithm of a measured spectrum I and a reference spectrum I_0:

$$\ln\frac{I_0(\lambda)}{I(\lambda)} = \sum_{i=1}^{k} \sigma_i(\lambda)\cdot S_i + \underbrace{\sum_{p=1}^{l} a_p \lambda^p}_{P} \quad (1)$$

Usually, the absorption due to trace gases shows a strong variation with wavelength λ. It is described by the absorption cross sections of the considered molecules that are known from laboratory measurements. Structures due to scattering, which vary only slowly with wavelength, are described by a broadband polynomial P (last term in Eq. 1) of order l in the fit analysis (Platt, 1994). The reference spectrum does not include the trace gas absorptions or only contains a small amount. For satellite observations usually a direct Sun spectrum, or – for satellite limb geometry – a spectrum measured at high tangent height (TH), where the considered trace gas has low concentration, is applied as reference spectrum. In a least squares fit, the differences between the right and left terms of Eq. (1) are minimized for all wavelengths providing as result the SCDs S_i and polynomial coefficients a_p that fit best to the respective measurement.

The SCD is related to the VCD being a product of AMF A_i and VCD V_i:

$$S_i = A_i \cdot V_i \quad (2)$$

Equations (1) and (2) are simplifications in so far as the wavelength dependency of AMF and SCD is not considered. For example in standard DOAS application for measurements of scattered light, the SCDs are considered as wavelength independent parameters. This simplification can be applied for a wide range of observation geometries and absorbers, as long as the dependency of the SCDs on wavelength is negligible within the fitting window. Therefore, the standard DOAS approach can be performed for many applications with only negligible errors due to the weak dependency of the SCDs on the wavelength.

AMTD
2, 2919–2982, 2009

2.1.2 Limitations for measurements of scattered light

For very long light paths or cases of strong absorption, however, it is found that the variability of the SCD in the fit window becomes important. For DOAS applications on satellite nadir geometry, this was first described by Diebel et al. (1995) and Richter (1997): For the retrieval of ozone VCDs from simulated spectra in a wavelength region between 335–346 nm, a discrepancy of ∼2% for SZA significantly below 90° and ∼15% for SZA near to 90° was found with respect to the true column.

The wavelength dependence of the SCD is caused by two effects:

(1) The slant path of scattered light varies with wavelength and the light path distribution changes (e.g. Solomon et al., 1987), since the Rayleigh-scattering cross-section varies as the inverse of the wavelength to the fourth power. Also, other scattering and reflection processes (on clouds, aerosols or ground) in the atmosphere are characterized by broad band functions from wavelength.

(2) SCDs vary across spectral structures of the trace gas absorption cross-sections because different light paths through the atmosphere also depend on the strength of the trace gas absorption (Platt et al., 1997; Marquard et al., 2000). Longer paths with stronger absorption have a smaller intensity and thus contribute less to the measurement than shorter paths with weaker absorption. The effect becomes more pronounced for stronger absorption and when light crosses the atmosphere along very different trajectories. In opposite to the broadband scattering effect, the wavelength dependence caused by absorption can have a narrowband component of SCD variation because it depends on the absorption cross-sections of the absorbing trace gases.

Thus, the assumption of a wavelength and absorption independent SCD may lead to errors in the detection of all trace gases analysed in a specific wavelength interval. In particular, neglecting the wavelength dependency for the strong absorbers will affect the retrieval of the minor absorbers. A more accurate description of the relation

AMTD
2, 2919–2982, 2009

between vertical and slant column density should therefore take into account also the dependency on wavelength and vertical optical depth υ (Marquard et al., 2000):

$$S_i = S_i(\lambda\upsilon) = A_i(\lambda\upsilon) \cdot V_i \tag{3}$$

For a number of k absorbers, the total vertical optical depth is the sum of the vertical optical depths of the individual absorbers:

$$\upsilon = \sum_{i=1}^{k} V_i \sigma_i \tag{4}$$

2.1.3 AMFs for strong absorptions in limb geometry

In limb geometry, light that is detected by the instrument arises from various locations along the LOS which has a length on the order of up to one thousand km through the Earth's atmosphere. Due to the wavelength dependency of the scattering and also the absorption processes, the length and the geometry of the trajectories of individual light paths differ significantly. As a result, the variation of the AMF (or the SCD) with wavelength for limb geometry is much stronger than e.g. for nadir geometry.

Examples of AMFs for the wavelength region of 332–357 nm are illustrated in Fig. 1 for nadir (left panel) and limb (right panel) geometry for predefined atmospheric scenarios (Parameters of the simulation are given in Table 1). Also the amplitudes of the AMF variation with respect to the mean value and their standard deviation are given in Table 2.

For nadir geometry at a SZA=75° (see the blue line in the left panel of the figure), a variation of the AMF in the fit window of about 3% is observed, with a slight increase towards longer wavelengths. Additionally, at wavelengths, where absorption by ozone is stronger (because of the increased ozone absorption cross-section), AMFs are decreased (by ~2% at 334 nm). For the SZA of 90° (green line), however, the increase for longer wavelengths is much stronger and the variation along the ozone absorption

AMTD
2, 2919–2982, 2009

bands is more prominent, resulting in a variation of the AMFs in the fit window of around 25%.

This strong dependency of the AMF on wavelength causes the discrepancies in the ozone retrieval described by Diebel et al. (1995) and Richter (1997).

Compared with nadir view, the variation with wavelength for limb geometry is one order of magnitude stronger for a scenario with SZA=75° and the ozone VCD of 460 DU (solid red and cyan lines in the right panel of the figure). The variation is around 25% with up to ∼10% decrease at the ozone absorption bands for a TH near to the peak of the BrO and ozone profile.

A clear dependency of the AMF of ozone on its optical depth is observed: For an ozone profile with a VCD of 460 DU (solid red and cyan lines in the plot) the AMFs decrease in comparison to the ozone profile scaled to a VCD of 200 DU (dashed red and cyan lines). The difference is stronger for those wavelengths where the absorption cross-section of ozone is larger. The ozone profiles applied for the simulations are plotted in Fig. 2.

Due to the long light paths for limb geometry and the resulting large differences of the light paths, the strong variation of the AMF with wavelength occurs already for low SZAs. For nadir geometry, however, the lengths of the light paths increase strongly only at high SZAs (i.e. at SZAs close to 90°). As a result, for nadir observations, only a small part of all satellite measurements is affected by large discrepancies. However, for limb geometry, every measurement is affected significantly. Therefore taking into account the wavelength dependency of the AMF is much more necessary for limb measurements than for nadir.

2.2 A new approach for accounting for the variability of SCDs and AMFs in the DOAS fit

In the following, we introduce a new approach to take into account the spectral dependency of the SCD or AMF on wavelength in the DOAS fit, and thereby to minimize the associated retrieval error. As summarized above (see Sects. 2.1.2 and 2.1.3), the

AMTD
2, 2919–2982, 2009

wavelength dependency of the SCD and the AMF results from the dependency on scattering and absorption processes (Eq. 3). Both processes can be described by a broadband function of wavelength and/or the optical depth (which itself shows a narrow band variation on wavelength). Thus, it is reasonable to formulate the SCD or the AMF as a function of wavelength and optical depth. The Taylor series expansion for such a function generally can be written:

$$F(\lambda,\upsilon) = \sum_{n=0}^{\infty}\sum_{m=0}^{\infty} \frac{\partial^n \partial^m}{\partial\lambda^n \partial\upsilon^m} \frac{F(w,d)}{n!m!} (\lambda - w)^n (\upsilon - d)^m \quad (5)$$

$F(\lambda,\upsilon)$ can be either the approximated SCD or AMF at wavelength w and vertical optical depth d. n and m is the order of derivation with respect to wavelength λ and vertical optical depth υ, respectively.

The basic spectral quantity in DOAS is the optical depth but it is possible to express it with respect to other spectral quantities (e.g. SCD or AMF). The mathematical relations for the spectroscopic quantities (SCD, VCD and optical depth) are summarized in Table 3. It is also possible to apply the Taylor series description specifically for any of these quantities considering their relations to Eq. (5). In the following they are given for SCD, AMF and optical depth.

2.2.1 First order approximation for the SCD

If taking into account the terms up to the 1st order, the wavelength and optical depth dependent SCD is described by:

$$S(\lambda,\upsilon)|_{n\leq 1, m\leq 1} = S_0(w,d) + S_\lambda(w,d)(\lambda - w) + S_\upsilon(w,d)(\upsilon - d) \quad (6)$$

In Eqs. (5) and (6) the broad band variations (caused by scattering and slowly varying absorption component) are described by the Taylor expansion with respect to wavelength, while the narrow band variations due to absorption are described by the Taylor expansion with respect to the vertical optical depth which varies with wavelength according to the narrow band absorption structures.

After grouping similar terms together, Eq. (6) results in:

$$S(\lambda,\upsilon)\approx S_0^*(w,d)+S_\lambda(w,d)\lambda+S_\upsilon(w,d)\upsilon \quad (7)$$

where:

$$S_0^*(w,d)=S_0-S_\lambda\cdot d-S_\upsilon\cdot w \quad (8)$$

When considering the vertical optical depths of several absorbers (compare with Eq. 4, the last term of Eq. 7), describing the dependency of the SCD on absorption, becomes:

$$S_\upsilon\upsilon=S_\upsilon\sum_{i=1}^{k}V_i\sigma_i=\sum_{i=1}^{k}\underbrace{S_\upsilon V_i}_{S_i}\sigma_i=\sum_{i=1}^{k}S_i\sigma_i \quad (9)$$

With this term it is possible to describe the absorption of each trace gas by the product of a constant S_i (later to be determined by DOAS) and its cross-section σ_i. Because the vertical optical depths of minor absorbers cause only negligible contributions to the total optical depth, it is necessary to consider the wavelength dependency of the SCD only for strong absorbers in practice. For example, in Sect. 3 we show that the DOAS retrieval of BrO is improved considerably when including the first order terms according to Eq. (7) for the ozone SCD in the spectral analysis (this first order approximation in the following is referred to as the Taylor series approach). However, taking into account the wavelength dependency of the SCDs also for minor absorbers, further improves the retrieval (see Appendix B).

2.2.2 First order approximation for the AMF

In analogy to Eq. (7) (taking into account the proportionality between SCD and AMF in Eq. 3), the first order approximation for AMFs is described by:

$$A(\lambda,\upsilon)\approx A_0^*+A_\lambda\lambda+A_\upsilon\upsilon \quad (10)$$

In Sect. 2.3 we show that the approximation of ozone AMFs by Eq. (10) results in an agreement with the true AMF dependency on wavelength, which is improved by one order of magnitude compared to the simplification of a constant AMF.

2.2.3 First order approximation for optical depth

In the DOAS equation, the optical depth of a particular trace gas is a product of Eq. (7) and its cross-section σ. Thus, the optical depth for an absorber according to Eq. (7) is:

$$\tau(\lambda,\upsilon)\approx S_0^*\sigma+S_\lambda\lambda\sigma+S_\upsilon\upsilon\sigma \tag{11}$$

Parameters S_0^*, S_λ and S_υ are functions at arbitrary wavelength w and vertical optical depth d and are determined by a common least squares DOAS fit. The total wavelength dependent SCD S of the considered absorber is then resulting from the Eq. (7).

If we consider only the absorption of the strong absorber and write Eq. (11) for the optical depth of this absorber, it becomes (considering only S_i in Eq. 9) for the strong absorber S_s only):

$$\tau(\lambda,\upsilon)\approx S_0^*\sigma_s+S_\lambda\lambda\sigma_s+S_s\sigma_s^2 \tag{12}$$

2.3 Approximation for the spectral variation of simulated AMFs of ozone in the UV spectral range for limb geometry

In order to take into account the wavelength dependency of the ozone AMF, we first perform a simple study to investigate if the Taylor expansion according to Eq. (10) is resulting in an improved description of the AMF for ozone (in comparison to assuming a constant AMF).

For the study, we simulated AMFs for limb geometry in the UV spectral region (338–357 nm), see "main" parameters given in Table 1. The AMFs are obtained by the RTM McArtim (Deutschmann, 2009) from the simulated spectral intensity with and without the ozone absorption (according to the second last row in the third column in Table 3). In this wavelength region, although the minor absorbers are present, the absorption by

AMTD
2, 2919–2982, 2009

ozone dominates. Therefore according to Eq. (10) the first order Taylor series expansion for the AMF of ozone is:

$$A(\lambda,\upsilon)\approx A_0^*+A_\lambda\lambda+A_{O_3}\sigma_{O_3} \quad (13)$$

The coefficients A_0^*, A_λ and A_{O_3} are fitted minimizing the difference between the right side of the Eq. (13) and the simulated (true) AMFs on the left side of it. In Fig. 3, the difference between the approximation by the Taylor series and the simulated values is plotted as mean for all THs (case a, blue line) in order to show the general effect. The agreement is better than ~0.4% for all wavelengths (the discrepancy is slightly higher for THs close to the peak of the BrO profile and lower above).

This means that with respect to the simplification of a constant AMF, where discrepancies of up to 20% arise for certain wavelengths (compare Fig. 1), the new approach has a maximum discrepancy of only 0.4% for the whole fit window.

In the case if the minor absorbers were not included in the simulation, the improvement would be even better (i.e. close to the Monte Carlo noise of the RTM simulation). But in reality they are present in the atmosphere. The small differences that remain (for example, at 338.5 and 355 nm) are due to the absorption bands of minor absorbers, which are included in the atmospheric scenario used for simulation studies (BrO and NO_2), and higher order structures with respect to wavelength and ozone absorption. They are not considered in the approximation by Eq. (13) due to the small effect on the total vertical optical depth and consequently on the AMFs of ozone.

However, including in the fit also the first order parameter A_{BrO} with respect to the absorption σ_{BrO} of BrO (i.e. adding additional term for the description of vertical optical depth in Eq. 9), an improvement by an additional order of magnitude at the strongest absorption band of BrO is achieved (case b, green line in Fig. 3). The included terms are listed in Table 4.

Furthermore, it is also possible to correct for the still remaining systematic effects by including also a term A_{NO_2} for NO_2 (case c, cyan line in the Fig. 3). An agreement close to the precision of the simulation noise is obtained when additionally including

AMTD
2, 2919–2982, 2009

the parameters for the second order terms for dependency on wavelength and the absorption of ozone ($A_{\lambda\lambda}$, $A_{\lambda O_3}$ and $A_{O_3O_3}$), see case d, red line.

From this level of agreement one may deduce that this Taylor series expansion does not neglect (in the extent of practical applicability) any systematic effects on the wavelength dependency of the AMF. On the other hand, the significantly improved description of the wavelength dependency of the AMF already by the first order Taylor series approach (Eq. 13) lets us expect that the inclusion of the first order terms in the DOAS retrieval will also lead to a significant improvement compared to the assumption of a constant SCD.

3 Application of the Taylor series approach in the DOAS retrieval for simulated spectra

Due to the improved AMF approximation by the new approach, the inclusion of the first order terms in the SCD retrieval by DOAS should lead also to much better results, meaning more accurate retrieved values and less systematic errors. In the following we apply the new retrieval approach performing the DOAS fit i.e. we retrieve SCDs of several absorbing trace gases (ozone, BrO and NO_2) from the simulated spectra.

For the study, we apply spectra simulated by the RTM McArtim with the same settings as used for AMFs approximation study (Table 1, the main settings), corresponding to the SCIAMACHY limb scanning sequence on 24 March 2003 over Kiruna with a SZA of 75° at the tangent point (TP). The output of the RTM is the sun normalized radiance i.e. $I//I_0$. The wavelength range of 338–357 nm, which is employed in our standard retrieval algorithm for BrO is used, for details see Kühl et al. (2008).

The standard DOAS approach for the absorption of ozone, NO_2 and BrO according to Eq. (1) is:

$$\ln\frac{I_0(\lambda)}{I(\lambda)} = S_{O_3}\sigma_{O_3}(\lambda) + S_{NO_2}\sigma_{NO_2}(\lambda) + S_{BrO}\sigma_{BrO}(\lambda) + P \qquad (14)$$

AMTD
2, 2919–2982, 2009

In the considered UV/VIS spectral range the absorption by ozone dominates. Taking into account the Taylor expansion terms of the first order for this strong absorber, the expression for the SCD according to Eq. (7) becomes:

$$S(\lambda,\upsilon)\approx S^*_{0,O_3}+S_{\lambda,O_3}\lambda+S_{O_3,O_3}\sigma_{O_3} \quad (15)$$

Where, according to Eq. (9) and neglecting the contribution of minor absorbers to the vertical optical depth the last term is:

$$S_{O_3,O_3}\sigma_{O_3}\approx S_{\upsilon,O_3}V_{O_3} \quad (16)$$

The second trace gas (i.e. O_3) term in the subscripts of Eqs. (15)–(16) and in the following equations indicates that the Taylor expansion is done for the SCD of ozone.

Equivalently for the DOAS application, the correction for the optical depth of ozone (being a product of the SCD and the absorption cross-section) becomes:

$$\tau_{O_3}(\lambda,\upsilon)\approx S^*_{0,O_3}\sigma_{O_3}+S_{\lambda,O_3}\lambda\sigma_{O_3}+S_{O_3,O_3}\sigma^2_{O_3} \quad (17)$$

The wavelength independent constant for the ozone SCD S_{O_3} in Eq. (14) is replaced by the Taylor series approach from Eq. (15), describing the wavelength dependency of the ozone SCD. In terms of the optical depth, however, the product of the wavelength independent SCD of ozone and its cross-section is replaced by the Taylor series approach for the optical depth from Eq. (17):

$$\ln\frac{I_0(\lambda)}{I(\lambda)}=S^*_{0,O_3}\sigma_{O_3}+S_{\lambda,O_3}\lambda\sigma_{O_3}+S_{O_3,O_3}\sigma^2_{O_3}+S_{NO_2}\sigma_{NO_2}(\lambda)+S_{BrO}\sigma_{BrO}(\lambda)+P \quad (18)$$

The common DOAS least squares fit of SCDs is performed minimizing the difference between the left and right side of the equation for all wavelengths. Slant column densities of NO_2 and BrO (S_{NO_2} and S_{BrO}) are fitted as constants in the study. The wavelength dependent SCD of ozone is acquired from the fitted coefficients S_{0,O_3}, S_{λ,O_3} and S_{O_3,O_3} by Eq. (15).

AMTD
2, 2919–2982, 2009

Alternatively for comparison we apply also the AMF modified DOAS method (according to Diebel et al., 1995; Richter, 1997) where the variation of the ozone SCD in the fit window is described by the AMF:

$$\ln\frac{I_0(\lambda)}{I(\lambda)} = \underbrace{V_{O_3} A_{O_3}(\lambda)}_{S_{O_3}} \sigma_{O_3}(\lambda) + S_{NO_2}\sigma_{NO_2}(\lambda) + S_{BrO}\sigma_{BrO}(\lambda) + P \quad (19)$$

Here the VCD of ozone is acquired directly by fitting the $A_{O_3}\sigma_{O_3}$ term (where the AMFs should be calculated for every wavelength in advance for an a-priori scenario). The SCD here is obtained as the product of the fitted VCD and the AMFs used for the fit.

The terms used for the description of the optical depth of absorption by the different approaches are summarized in Table 5.

3.1 Improvement for the retrieval of ozone SCDs

In the following, we describe that the new Taylor series approach considering the wavelength dependency of the SCDs of ozone (Eq. 18) results in an improvement for the fit of SCDs of ozone and thereby also for the fit of the weak absorber BrO (Sect. 3.2).

Figure 4 shows the relative deviation of the fitted SCDs of ozone from the true values simulated by the RTM for selected THs (near to the peak of the BrO profile - at 19.8 and 22.8 km). Included are the results for the Taylor series approach, the standard DOAS and the AMF modified DOAS. For the Taylor series approach, the wavelength dependent SCD of ozone is acquired by Eq. (15).

The standard DOAS approach, which neglects the variation of the ozone SCD in the fit window, gives more than 10% underestimation with respect to the true values of the SCDs (dashed lines in Fig. 4). This difference reflects the variability of the AMFs in the fit window, discussed in the section before. The discrepancy is largest at longer wavelengths (outside the strong absorption bands) because the DOAS fit is

AMTD
2, 2919–2982, 2009

constrained more by the wavelength regions with the strongest variations of the cross-section (e.g. Marquard et al., 2000).

In comparison, the novel approach for the parameterization of the SCDs of ozone by the Taylor series approach improves the description of SCDs of ozone significantly (see solid lines in Fig. 4): the deviation from the true value is only 1.5% at maximum at the longer wavelength edge of the fit window as can be seen in the figure. Similarly as for the description of the AMFs in Sect. 2.3, the improvement for the SCDs retrieved from the simulated intensities is one order of magnitude, compared with the standard approach. Thus, these results indicate that the approach allows to account much better for the variation of SCD of ozone in the fit window, even without knowledge of the ozone AMFs. The remaining negative discrepancy and structures at BrO absorption peaks in the figure can be explained by unfitted higher order terms and the impact of minor absorbers on the ozone SCD.

The AMF modified DOAS (the retrieved SCD for this method is a product of fitted VCD and the AMFs included in the fit) also gives a good agreement of 0.5% (see dotted lines in Fig. 4). The small disagreement probably arises from the interference with the absorption structures of the minor absorbers because the variation of their SCDs with wavelength is not accounted in the fit. Note that for this retrieval AMFs calculated for the same parameters as the model scenario were applied. Therefore in real applications where the atmospheric scenario is not known beforehand larger discrepancies may be expected.

Although the value for the SCD retrieved by standard DOAS shows more than 10% difference in particular for the longer wavelengths of the fit window, it agrees better with the true SCD for wavelengths around 340 nm near the strongest absorption peaks of ozone. In this region the error is less than 2% or even an agreement is found between retrieved and simulated values. The wavelengths at which the agreement is found may vary for different scenarios and generally cannot be extrapolated to every scenario. However, by applying the AMF evaluated in this wavelength range, a rather accurate ozone profile can be retrieved. Thus the introduced Taylor series approach would not

AMTD
2, 2919–2982, 2009

always be necessary for the ozone retrieval although the retrieved Taylor series terms may improve it substantially especially when appropriate wavelength range for the retrieval is used and iterative schemes are applied. However, the unfitted absorptions due to ozone will cause large errors in the retrieval of minor absorbers as is shown in detail in the following section.

3.2 Improvement for the retrieval of BrO

The improved description of the optical depth of ozone (by accounting for the wavelength dependent SCD of ozone) in the BrO DOAS analysis leads to a more correct retrieval of the SCD or optical depth of ozone as was shown in the previous section. In the following, we show that this improvement in the ozone SCD retrieval also results in a much better agreement of the retrieved BrO vertical profile with the true simulated profile (compared with standard DOAS).

3.2.1 Slant column density of BrO

For the same scenario and spectra as in Sect. 3.1, we now investigate the retrieved values of BrO. SCDs of BrO retrieved for the three approaches (i.e. standard DOAS, Taylor series approach for the SCDs of ozone, and AMF modified DOAS for ozone) are depicted in Fig. 5 (left panel). The values for standard DOAS (green line) are by up to 15% larger in comparison with the Taylor series approach (red line) as well as with AMF modified DOAS (magenta line). This can be explained by unfitted structures in the fit residual (see Fig. 6) that increase the retrieval error for the standard DOAS approach: As illustrated in Fig. 6, residual structures around the ozone absorption bands occur because of not accounting for the variation of the SCD of ozone in the fit window. These ozone specific absorption structures remain because they are not (completely) allocated to other fit parameters. However, misallocation of some optical depth of ozone to BrO takes place: The underestimation of the SCD (or optical depth) of ozone at the absorption bands of BrO (compare e.g. SCD of ozone at 338 nm, where

the strongest BrO absorption band occurs, in Fig. 4) leads to an overestimation of the retrieved SCDs of BrO in the standard DOAS. This dependency of the retrieved BrO SCDs on the ozone absorption is investigated in more detail in Appendix B.

On the other hand, the SCDs of BrO retrieved by the Taylor series approach or AMF modified DOAS (for SCD of ozone) agree well with the simulated BrO SCDs (which are determined by RTM from the intensity by the relation given in Table 3 similarly as for the ozone SCDs) at wavelengths close to the strongest absorption peaks of BrO and have only negligible impact from ozone absorption as shown in the Appendix B. The residual structures are reduced by one order of magnitude (see Fig. 6, bottom panel). Therefore also the error of the fit is reduced significantly. The reason for these improvements is that the optical depth variation of ozone is described better for the whole fit window. For the AMF modified DOAS, the improvement in describing the spectral structures is very similar as for Taylor series approach.

3.2.2 Improvement for the retrieved BrO profile

In the next step, the BrO profile is determined by inversion of the BrO SCDs. For this purpose, we apply our general retrieval algorithm based on the linear optimal estimation method (Rodgers, 2000) and described in detail in Puķīte et al. (2006) and Kühl et al. (2008). The a-priori settings are selected assuring that the measurement response (i.e. the sum of the rows of the averaging kernel matrix) is near to one at the altitudes above 13 km for all of the approaches (the standard DOAS, the Taylor series approach and the AMF modified DOAS). To achieve this, an a-priori profile as 2/3 of the true profile is used, with an a-priori uncertainty of 100% of its maximum value. The retrieval is performed on a 1 km grid. For smoothing purposes, a correlation length (see Rodgers, 2000, page 38) of 3.5 km is introduced in the a-priori covariance matrix. With these settings, the impact of the a-priori is minimized for this altitude range so that even a shift of the a-priori profile by 3 km downwards results in less than ~2% fluctuations in retrieved profiles both for the Taylor series approach and AMF modified DOAS, and less than ~5% changes for the standard DOAS.

AMTD
2, 2919–2982, 2009

In order to limit the systematical retrieval error to algorithm constraints only, the box AMFs for the inversion are calculated for the same atmospheric condition as the simulated spectra. Box AMFs applied for the inversion are derived by a weighted average of box AMFs calculated at different wavelengths based on an approach provided in Marquard et al. (2000) that the fit procedure is constrained stronger by absorption structures that vary more rapidly with wavelength. An alternative retrieval is performed with box AMFs calculated at a single wavelength of 344.2 nm. At this wavelength, the retrieved BrO SCDs agree with the true SCDs of BrO within ~3% for different ozone profiles as it is deduced from sensitivity studies, see e.g. Fig. 12, second panel from top, in the Appendix B.

The obtained vertical concentration profiles are depicted in Fig. 5 (middle panel) together with the true profile. The profile retrieved from SCDs acquired by standard DOAS shows a shift upwards (by ~1.5 km) and increased values at the peak by ~10% (see difference plots between the retrieved profiles and the true profile in Fig. 5, right panel). The overestimation above the peak is even more than 20 or 25% for altitudes where the ozone concentration is still very large, i.e. around 20 km (compare with Fig. 2). The profile obtained by the AMF modified DOAS or the Taylor series approach agrees much better with the true profile used for the simulation. For altitudes between 15 and 28 km the agreement for the Taylor series approach is better than 5%. For altitudes below 15 km the discrepancy increases to ~10% (note that below 12 km the measurement response is very low).

Thus, although the SCDs of minor absorbers vary in the fit window because they depend on wavelength and the absorption of strong absorbers, it is shown that the retrieval of the BrO is improved considerably if the variability of the SCD of ozone in the fit window is considered.

For the AMF modified DOAS, the disagreement around altitudes of 19 km and also the slightly lower values for the Taylor series approach probably arise from the interference with the absorption structures of the minor absorbers (note that the AMF modified DOAS and also the Taylor series DOAS are performed only for the SCD of ozone).

AMTD
2, 2919–2982, 2009

In Fig. 5 also the profile obtained by inversion of the SCDs acquired by the Taylor series approach applying the box AMFs at the selected single wavelength (344.2 nm) is plotted (red dashed line). This also shows an overall good agreement within 3% for most altitudes (compare also sensitivity studies in the Appendix B).

It should be noted that all discussed methods can use an iterative schema in order to improve the profile retrieval. Thereby the a-priori knowledge for quantities to be retrieved can be updated in the next iteration. Thus retrieved information can be used in the next iteration step for calculation of AMFs or weighting functions.

4 Sensitivity studies (for simulated spectra)

The previous section revealed that the retrieval both for ozone and for the minor absorber BrO can be improved significantly for the fit window of 338–357 nm by the Taylor series approach (first order terms with respect to wavelength and absorption): The agreement with the true (simulated) values and also the fit quality can be improved by minimizing the fit residual. This was studied for a subarctic atmospheric scenario with a relatively strong absorption of ozone with the VCD of 460 DU.

In this section we investigate the retrieval for different fit windows within the wavelength range of 332-357 nm, considering different BrO absorption bands, see Sect. 4.1. In Sect. 4.2, the sensitivity of the retrieval of BrO is studied for different absorption strengths of ozone and BrO by assuming different atmospheric profiles.

Additionally, in the Appendix B, we provide a study for the capability to describe also SCDs of the minor absorber BrO by Taylor series terms.

AMTD
2, 2919–2982, 2009

4.1 Application of the method for different fit windows

Since the strength of absorption and the scattering probability in the atmosphere vary with wavelength, the improvement of the Taylor series approach with respect to the standard DOAS may be different for fit windows covering various wavelength ranges. Also the different terms of the Taylor series approach (with respect to wavelength or ozone absorption, see Eq. 17) will impact the BrO profile retrieval differently from one fit window to another.

We investigated the applicability of the approach for different fit windows in the range of 332-357 nm where BrO absorption is largest. For this study, we extended the spectral region for the simulation of spectra with respect to the main settings in Sect. 3 including one additional BrO absorption band at shorter wavelengths (see Fig. 7 where the BrO cross-section used in this study is plotted) compared with the fit window applied before.

We performed the DOAS retrieval of SCDs considering various parameters of the Taylor series: The calculations are performed including either all three terms in Eq. (17) or when only the broadband wavelength dependency is accounted for (by the first and the second term in the equation) or when only the narrow band dependency due to the ozone absorption structures is considered (by the first and the third term). As comparison, we also applied the standard DOAS retrieval. In the Appendix A, the equations for the different DOAS approaches and the calculation of the SCDs from the fitted parameters are given (Eq. A1-A4). Also, the impact on the ozone SCD is explored for the fit window of 338–357 nm in Appendix A.

The study is performed for (all possible combinations of) fit windows with 2-5 BrO absorption peaks. The fit windows studied and the BrO profiles retrieved are depicted in Fig. 8 as well, the comparisons of the quality of the retrieved profiles by the different methods are described in Table 6.

Standard DOAS: Summarizing the results, standard DOAS (green lines in the Fig. 8) gives better results for fit windows that do not include the first absorption peak of BrO

AMTD
2, 2919–2982, 2009

at 334 nm because otherwise large retrieval errors (due to large structures in the residuals) are obtained. For cases if only two absorption bands are considered (the last plots on the right), the error decreases if the bands at higher wavelengths are included in the fit because of the decrease in the ozone absorption. Therefore only for the fit window 347.8-357 nm (see the plot in the bottom panel), a very good agreement for standard DOAS application is obtained.

Taylor series approach: It improves the retrieved BrO profile (red lines in the Fig. 8) compared with the standard DOAS considerably. It shows only some small discrepancies (not much larger than 5%) for the fit windows starting at shorter wavelengths probably because of the effect of minor trace gases on ozone absorption.

The agreement is even better either for very large fit windows (332-357 nm and 332-351.1 nm, first and second plots from left at the top in the figure) or for fit windows at longer wavelengths where the ozone absorption is smaller (those starting at 341.3 nm, see last two panels at the bottom in the Fig. 8).

Separate terms of Taylor series approach: Some improvement is gained with respect to the standard DOAS already if only either the wavelength dependency term ($S_{\lambda,O_3}\lambda\sigma_{O_3}$) or cross-section dependency term ($S_{O_3,O_3}\sigma^2_{O_3}$) for the optical depth of ozone is included in DOAS (black and brown lines in Fig. 8, respectively). In particular, a good agreement with the true profile is found for the cases when only the wavelength term is considered for the fit windows with the lower boundary at or above 338 nm (see plots in the last tree panels from the top in the figure). For fit windows including the much stronger ozone absorption band at 334 nm (plots in the top panel), however, the consideration of the cross-section term in describing of ozone SCDs is important in order to retrieve correct values of BrO concentration. Neglecting this term can lead to errors of up to 20%.

Summarizing, the Taylor series approach allows to extend the application of DOAS for any studied fit window without the necessity to account for a-priori information for the AMF calculation that in general may differ from reality especially regarding scattering processes in the atmosphere (e.g. clouds, aerosols, temperature and pressure).

AMTD
2, 2919–2982, 2009

For the studied fit windows we also retrieved the BrO profile with AMF modified DOAS. The agreement with the Taylor series approach is within 5% for altitudes between 15 and 25 km except for the fit window of 332.02-339.94 nm where only the first two BrO absorption peaks are accounted in the fit and the Taylor series approach gives by ∼10% lower values for altitudes above the peak compared with AMF modified DOAS and the true profile.

4.2 Application of the method for different atmospheric conditions

In the previous section, the effect of the Taylor series approach for the wavelength dependency of the ozone SCDs in the DOAS fit was investigated for one predefined atmospheric condition with large absorption of ozone (TC=460 DU) and a SZA of 75°, according to the main settings in Table 1. In this section, the performance of the approach is investigated for different atmospheric conditions.

Of particular interest is the response of the approach to different ozone profiles. We found in case studies that other atmospheric parameters that impact the light distribution in the atmosphere (different temperature, pressure, as well as viewing geometry) have very small effect compared with the effect caused by the ozone absorption.

In the study of the impact of the ozone absorption, we investigate: (1) the effect of different vertical optical depth of ozone on the retrieval of BrO by scaling the ozone profile, and (2) the effect of a different ozone profile with the concentration peak at higher altitudes. For simulations of spectra we apply the ozone profiles as indicated in Fig. 2 and Table 1: In the first case, for the subarctic scenario, the ozone profile with VCD=460 DU is scaled to 200 DU. In the other case, for tropical scenario, besides applying the ozone profile characteristic for tropics (VCD=270 DU, the profile peak at higher altitude, i.e. at 28 km), also the subarctic profile (with peak at 18 km, scaled to 200 DU) is applied for spectra simulations.

The retrieved BrO profiles and their comparison are given in Fig. 9.

When the ozone profile is scaled to 200 DU, an overall better agreement for the retrieved profile of BrO with the true profile is obtained both for the standard DOAS

AMTD
2, 2919–2982, 2009

and for the Taylor series approach than for the ozone profile with VCD=460 DU (see Fig. 9, left panel): For the standard DOAS, for most altitudes the agreement is within 10% (see the difference plots in the second panel from left in the figure). For the Taylor series approach, the agreement is within 2% between 16 and 30 km, with lower discrepancies for the ozone profile corresponding to 200 DU. Similarly to the standard DOAS, this can be explained by the decreased contribution of the ozone optical depth to the total optical depth of absorption. Therefore also the effects of not corrected higher order Taylor series terms and the impact of minor absorbers on the absorption of ozone decrease relatively to the total optical depth.

For the tropical scenario (Fig. 9, first two panels on the right) even larger relative discrepancy (up to 40%) in the retrieved profiles of BrO by the standard DOAS (see the solid green line in the plot) can be seen than for the scenarios studied before. The larger relative discrepancy (the same line in the plot in the figure on the right) can be explained by the lower BrO concentration. The absolute discrepancy, however, is similar to the scenario with the subarctic profile of ozone scaled to 200 DU. The largest discrepancy is observed for higher altitudes (above 25 km), compared with the subarctic scenario near Kiruna studied previously, because the ozone concentration peaks at higher altitudes (28 km) in the tropics (Fig. 2). This becomes clear by including in the comparison also a study where the tropical ozone profile is replaced by the subarctic ozone profile scaled to 200 DU which peaks at lower altitudes (19 km). For the latter, the largest disagreement of 20% is found at lower altitudes (below 20 km), i.e. near to peak of the particular ozone profile as indicated in Fig. 9 (see the dashed green line in the right plot in the figure).

The absolute difference between the BrO profile, retrieved with the Taylor series approach, and the true profile is similar for the cases with the tropical and the subarctic profile (the later scaled to VCD of 200 DU) because the ozone profile for the tropics has a similar VCD (i.e. 270 DU). In relative values, the discrepancy for the tropical profile is lower than 5% for altitudes above 20 km, but increases for altitudes below.

AMTD
2, 2919–2982, 2009

5 Application of the method to SCIAMACHY measurements

In the previous two sections, we showed the advantage of the Taylor series approach to improve the retrieval of BrO vertical profiles from simulated spectra. In this section we study the possibility to apply the method for the retrieval of BrO vertical profiles from SCIAMACHY limb measurements. We perform the retrieval of SCDs from measurements of SCIAMACHY both with standard DOAS and with the Taylor series approach and compare the retrieved vertical concentration profiles with correlated balloon measurements provided in Dorf et al. (2006, 2008).

5.1 Instrument description

The SCIAMACHY instrument on the ENVISAT satellite operates in a near polar sun synchronous orbit with an inclination from the equatorial plane of ~98.5°. It performs one orbit in approximately 100 min with equator crossing time of 10:00 in descending node. The satellite probes the atmosphere at the day side of Earth in alternating sequences of nadir and limb measurements. Limb scans in one scanning sequence are performed with approximately 3.3 km elevation steps at the TP in flight direction. The cross track swath is 960 km at the TP and consists of up to 4 pixels for the UV/VIS spectral range. The field of view (FOV) is 0.045° in elevation and 1.8° in azimuth. This corresponds to approximately 2.5 km in vertical direction and 110 km in horizontal direction at TP, respectively. SCIAMACHY measures in the UV-VIS-NIR spectral range from 240 to 2380 nm with a spectral resolution of approximately 0.25 to 0.55 nm in the UV-VIS range. More instrumental details can be found in Bovensmann et al. (1999).

AMTD
2, 2919–2982, 2009

5.2 Retrieval of BrO

For the retrieval of BrO vertical profiles from SCIAMACHY limb measurements, an algorithm developed in our group is applied (Kühl, 2005; Puķīte et al., 2006; Kühl et al., 2008). The retrieval of vertical BrO profiles from the SCIAMACHY limb spectra is done in two steps in a similar way as it is applied for the simulated spectra studies above.

In the first step, for the standard DOAS approach we apply the same retrieval settings as described in Kühl et al. (2008). The fit window ranges from 338.01–357.25 nm and two ozone cross-sections (at 223 and 243 K) are included in the fit in order to account for the ozone cross-section dependency on temperature.

For the Taylor series approach we implement the description of wavelength and absorption dependency of the ozone SCD in the fit window in the same way as for simulated spectra, i.e. replacing the standard DOAS approach by the three terms as in Eq. (18). Replaced is the ozone cross-section term at 223 K. The second cross-section term at 243 K is left unchanged as the task of it is to account for the dependency of the ozone cross-section on temperature. (We performed studies on simulated spectra with temperature dependent ozone cross-section and found that the spectral features of ozone absorption due to temperature is well accounted for already with this one additional term. Expansion of it in the Taylor series does not give additional improvement. Also orthogonalization of the ozone cross-section of 243 K with respect to the cross-section of 223 K does not impact the retrieval.) Alternatively we studied possibility to use the ozone cross-section at 203 K as the second term. We found that it gives better results for cases with colder temperatures.

For the second step of the retrieval, the inversion of the BrO SCDs to a number density profile of BrO, we apply the RTM "McArtim" (Deutschmann, 2009), like for the simulations above. Box AMFs according to the geometry of each individual SCIAMACHY measurement are calculated at the single wavelength of 344.2 nm (similarly as for the example in Sect. 3.2.2, see dashed red line in Fig. 5). In case studies we found that for this wavelength the retrieved and the true SCDs agree within ~3% for

AMTD
2, 2919–2982, 2009

different ozone profiles (see e.g. Fig. 12, second panel from top, in the Appendix B). Thus with this practical solution it is not necessary to calculate the box AMFs at all wavelengths which would be a very time consuming task for every SCIAMACHY measurement. The inversion is performed by the optimal estimation method (Rodgers, 2000). It is performed on the measurement grid with an a-priori variance of 100% and the off-diagonal elements of the covariance matrix being zero.

5.3 Comparison of SCIAMACHY BrO measurements with collocated balloon measurements

A number of balloon measurements were performed to validate the SCIAMACHY instrument (e.g. Butz et al., 2006; Dorf et al., 2006). The BrO profiles taken for this study were acquired from direct solar spectra measurements by LPMA/DOAS (Dorf et al., 2006). A photochemical correction and air mass trajectory modelling was performed for the balloon measurements in order to match the same place and atmospheric conditions (SZA) as for SCIAMACHY (except for the measurement at Teresina where only air mass trajectory modelling was performed). For the backward and forward trajectory modelling and for further information on the balloon measurements and the profile retrieval please refer to Dorf et al. (2006, 2008).

In Fig. 10, the BrO profiles retrieved by SCIAMACHY are compared with the correlated balloon observations for three different places: Kiruna (67.9° N, 21.1° E), Aire sur l'Adour (43.7° N, 0.3° E) and Teresina (5.1° S, 42.9° W) and for three different seasons (March, October and June). The altitudes where the modelled trajectories of air masses measured by balloon match with the TPs of SCIAMACHY limb observations are indicated in grey in the figure.

In comparison to the simulation study larger errors are expected for real measurements. These include effects of the temperature dependency of cross-sections, the spectral calibration, the Ring effect and instrumental problems. Also trajectory

AMTD
2, 2919–2982, 2009

modelling and photochemical correction for balloon measurements contributes to additional uncertainties in the comparison.

For most altitudes where the air masses measured by balloon and SCIAMACHY match, an overall good agreement within the error bars is found between SCIAMACHY BrO profiles retrieved by the Taylor series approach and the balloon BrO profiles. The agreement is within around 25% for both Kiruna cases (first and third panel from the top) and the observation at Aire sur l'Adour in France (second panel from the top).

There is a tendency for larger values in the SCIAMACHY BrO profiles for most of the cases. Note that for the balloon profile retrieval, the BrO cross section measured by Wahner et al. (1988) is used, while for the SCIAMACHY retrieval we apply the more recent one from Fleischmann et al. (2004). The cross-section by Wahner et al. (1988) has a coarser spectral resolution (~0.4 nm) than the SCIAMACHY spectra (~0.2 nm in the considered spectral region) therefore it is not appropriate for the SCIAMACHY BrO profile retrieval. However by convolving and fitting the cross-section by Fleischmann et al. (2004) to the resolution of the cross-section by Wahner et al. (1988) we found that the latter one is by ~10% larger in the fit window used for the balloon profile retrievals (346–360 nm). Therefore, by a similar factor higher concentrations would be expected to be retrieved from the balloon if they were analysed using the Fleischmann et al. (2004) cross section. (Reconsider that the DOAS retrieval determines the optical depth of the species, which is the product of the cross-section and SCD, see Table 3. Thus for larger cross-sections smaller SCDs are retrieved and vice versa.). Also, to investigate the uncertainties due to different BrO cross-sections on the SCIAMACHY BrO profile retrieval, it is alternatively performed with the cross-section measured by Wilmouth et al. (1999) (red dashed line). Because it is larger by ~10% compared with the cross-section by Fleischmann et al. (2004) but agrees with the cross section measured by Wahner et al. (1988) in the balloon fit window, the retrieved SCIAMACHY SCDs and consequently also profiles are lower by up to ~10% with respect to the retrieval with the cross-section by Fleischmann et al. (2004), however it agrees better with the balloon profiles.

AMTD
2, 2919–2982, 2009

Profiles retrieved from the SCDs acquired by standard DOAS generally show larger values compared with the Taylor series approach and also with respect to the balloon profiles.

The difference between both retrievals is the largest for measurements at Kiruna, where it is up to 25% for altitudes between 20 and 25 km. Also the discrepancy of the standard DOAS retrieval to the balloon profiles is significant (up to ∼40%). Note that for these days in March very large ozone columns (above 400 DU) were observed at Kiruna. Therefore the large discrepancy between the profiles obtained by standard DOAS and the Taylor series approach at the altitudes of the ozone peak may be attributed to the impact of the ozone absorption, which causes the overestimation of the BrO SCD for standard DOAS (compare simulation studies).

In contrast, for the observation above Aire sur l'Adour in October, the difference between both SCIAMACHY retrievals is smaller (between 10 and 15%) because of much smaller ozone columns (below 300 DU) observed compared with Kiruna. Thus, the impact of ozone absorption on the BrO retrieval is less and already the standard DOAS shows a good agreement with the balloon observation here.

For the tropical scenario over Brazil the standard DOAS gives 15-25% larger values compared with the Taylor series approach. The discrepancy is larger for altitudes above 25 km in accord to with the sensitivity studies for the tropical scenario (see Sect. 4.2).

The comparison at Aire sur l'Adour shows systematically lower values for SCIAMACHY at lower altitudes than for the balloon observations. Here very long trajectories (738–988 km), in opposite to other examples (being not larger than 500 km), was modelled in order to mach the SCIAMACHY measurements. We also found that for this scenario larger (by ∼5%) SCDs and concentration values are retrieved (see cyan line in the comparison plot for Aire sur l'Adour in Fig. 10) if the second ozone cross-section at 243 K (which is used besides the cross-section at 223 K in the fit) is replaced with the ozone cross-section at 203 K. We performed the retrieval with this setting for the ozone cross-sections also for the other cases but there no significant effect on the retrieved BrO profile was found. However, considering these findings we plan in the

AMTD
2, 2919–2982, 2009

future to study them in more detail and modify our retrieval algorithm in order to allow a more flexible selection of ozone cross-sections in the retrieval basing on the actual temperature in the atmosphere.

For the tropical case (bottom panel), significantly lower values are observed by up to 35% compared with the balloon observation for altitudes below 25 km. However for this case, also other retrieval algorithms retrieve lower concentrations from the SCIAMACHY measurements (Alexei Rozanov, personal communication, 2009). Beside the comparisons studied above, also other balloon measurements were performed; comparison with them is planned to be presented in a publication by Rozanov et al. (2005), where also BrO profiles retrieved from SCIAMACHY measurements by algorithms of other working groups will be included. Note that for all compared BrO profile retrievals the agreement with the profiles obtained by the IUP Bremen global fit approach (Rozanov et al., 2005) is improved when applying the Taylor series approach compared to standard DOAS.

6 Conclusions

For complex measurement geometries like satellite limb measurements, the light propagation in the atmosphere strongly varies with wavelength and the light can reach the instrument along very different light paths including those with strong absorption (e.g. due to ozone in the UV/VIS spectral range). Therefore the Lambert-Beer law is not applicable and the simplification of a constant SCD inside the DOAS fit window will lead to significant systematic errors.

For such cases, modifications for DOAS can be introduced accounting for the variability of the SCD in the fit window (e.g. extended or AMF modified DOAS). We introduced a new approach that describes the SCD as function of wavelength and of vertical optical depth (accounting for the broad band variation with wavelength because of changes in light propagation and absorption and also considering the narrow band dependency from absorption varying with cross-section, respectively). The functional

AMTD
2, 2919–2982, 2009

relationship is expressed in a Taylor series of which the first order terms are included in the DOAS fit allowing to account for the wavelength dependency of the SCD. Thus, wavelength dependent SCDs are determined by DOAS.

Applying the Taylor series approach on the SCIAMACHY limb observations more correct BrO profiles can be retrieved (compared with the standard DOAS approach). At the same time, the advantages of a two step approach are kept - radiative transfer is separated from spectral analysis, saving calculation time for both steps. In particular, box AMFs can be calculated at one selected single wavelength.

Studies based on simulated spectra demonstrated the usefulness of the method for different spectral regions in the range of 332–357 nm where relatively strong absorption by ozone prevail in the fit window and light path distribution in the atmosphere considerably changes with wavelength. Here, neglecting the dependency of ozone SCDs on wavelength leads to significant cross-effects on the retrieval of minor absorbers like BrO: Depending on the fit window the discrepancy to the true profile can reach 20 to 100%.

Accounting for this variation by the Taylor series approach provides a more correct retrieval of minor absorbers eliminating biases that arise due to the assumption of the constant ozone SCD in the fit window: Sensitivity studies show that the agreement between retrieved and simulated (true) BrO SCD is very similar for atmospheric scenarios with different ozone profiles. Also very good agreement between the retrieved and the true profile is found for different fit windows and ozone profiles.

We applied the Taylor series approach for retrieval of BrO profiles from SCIAMACHY measurements and compared the profiles with standard DOAS retrieval and correlated balloon measurements. While the profiles obtained by standard DOAS show discrepancies of up to ~40% compared to the balloon validation measurements, the Taylor series approach leads to much better agreement, in particular for cases with strong ozone absorption. This confirms the results of the sensitivity studies where an overestimation of the BrO SCD due to an incorrect ozone SCD description by the standard DOAS was found.

AMTD
2, 2919–2982, 2009

With respect to AMF modified DOAS Taylor series approach has the advantage of being independent from a-priori information that in general differs from reality. In addition it is not necessary to calculate AMFs for every wavelength in the fit window.

For the inversion of the SCDs to vertical profiles, the new approach makes the selection of wavelength much easier because the interference of the narrow band spectral features caused by the wavelength dependency of the SCD of strong absorbers with minor absorber is minimized. Therefore the selection of the wavelength at which the box AMFs for the inversion should be calculated depends much less on the strength of the absorption of ozone.

We demonstrated the improvement for the BrO profile retrieval with the Taylor series expansion for SCDs of ozone. However, the approach has the potential to improve DOAS retrievals also for other minor or strong absorbers when strong absorption is present in the atmosphere. In general, the approach allows to extend the applicability of DOAS for observations where the light path varies strongly with wavelength (e.g. limb measurements or scenarios with large SZAs for nadir, ground based or other observations) or where medium or strong absorptions occur, like e.g. ozone in the UV spectral range. Due to the improved description of the wavelength dependency of the SCDs, the Taylor series approach also allows to use broader fit windows which could improve the extraction of signals of very weak absorbers.

Appendix A

Sensitivity to different terms of the Taylor series

In the following, we investigate the quality of the retrieval when accounting for either only the broadband (due to scattering and absorption) or narrow band (due to ozone absorption) variation of SCDs of ozone in the fit window.

First, we include in the comparison the results when only the broadband dependency of the ozone SCD on wavelength is considered in the DOAS fit, but neglecting the

AMTD
2, 2919–2982, 2009

term describing the dependency on the ozone cross-section. The last is skipped in comparison to Eq. (18):

$$\ln\frac{I_0(\lambda)}{I(\lambda)} = O_3^* \sigma_{O_3} + S_{\lambda,O_3}\lambda\sigma_{O_3} + S_{NO_2}\sigma_{NO_2}(\lambda) + S_{BrO}\sigma_{BrO}(\lambda) + P \quad \text{(A1)}$$

In this case, the wavelength dependent SCD of ozone can be calculated from the fitted parameters in the following way:

$$S_f(\lambda) = S^*_{0,O_3} + S_{\lambda,O_3}\lambda \quad \text{(A2)}$$

Alternatively, the wavelength dependency of the SCD of ozone is considered only with respect to the spectral features of ozone absorption, neglecting the term describing the dependency on wavelength which is skipped in comparison to Eq. (18):

$$\ln\frac{I_0(\lambda)}{I(\lambda)} = S^*_{0,O_3}\sigma_{O_3} + S_{O_3,O_3}\sigma^2_{O_3} + S_{NO_2}\sigma_{NO_2}(\lambda) + S_{BrO}\sigma_{BrO}(\lambda) + P \quad \text{(A3)}$$

In this case, the wavelength dependent SCD of ozone is expressed by:

$$S_f(\lambda) = S^*_{0,O_3} + S_{O_3,O_3}\sigma_{O_3} \quad \text{(A4)}$$

We compare the ozone SCDs retrieved by the different approaches with the true SCDs. Figure 11 shows the deviation of the retrieved SCDs from the true values simulated by RTM. For this study, the same atmospheric and trace gas profiles as in the previous section (the main settings in Table 1), as well as the same fit window of 338–357 nm are applied.

Besides the observed error of up to 15% by the standard DOAS (the green line in the figure) and the improvement by one order of magnitude for the Taylor series approach (the red line in the figure), as discussed previously, significant uncorrected ozone structures are observed in the fit also for both approaches studied here. For the case when the ozone cross-section term is skipped, but the wavelength variation is accounted for, negative deviations of up to ~5% occur, which are stronger for THs

AMTD
2, 2919–2982, 2009

near the ozone peak (see blue dashed line in the figure). The agreement improves for larger wavelengths outside the strong absorption structures of ozone. For the second case (cyan dashed line in the figure) when the wavelength term is skipped, an offset in the range of 5 to −5% is observed with better agreement at the absorption peaks of ozone, however strong variations with wavelength in the fit window remain, i.e. it is only poorly improved against the standard DOAS. Also unfitted spectral structures of the ozone SCD remain in the fit residual.

Our studies show that neglecting one of the first order correction terms for ozone (broad band or ozone absorption) leads to poor results for the retrieval of the ozone SCD. However, for the retrieval of the BrO profile, there are only slight deviations found for the selected wavelength range of 338–357 nm and the studied atmospheric scenario (for more details, see Sect. 4.1 and second panel from top, left plot in Fig. 8).

Appendix B

Comparison between retrieved and true BrO SCD for different DOAS fits

Herein the retrieved SCDs of BrO are compared with the simulated (true) SCDs by RTM for the fit window 338–357 nm. The comparison is performed for standard DOAS, the Taylor series approach for the SCD of ozone, and the AMF modified DOAS for the SCD of ozone. Additionally the Taylor series approach is implemented for the SCD of BrO. Thus, four different approaches for the BrO DOAS fit are investigated, for details see Table 7, where the fit arguments for the SCDs of ozone and BrO and the equations for the calculation of the BrO SCDs are given. Fig. 12 shows the differences between the retrieved SCDs of BrO and the true SCDs as function of TH and wavelength for two different ozone profiles (the subarctic scenario with (a) the VCD=460 DU and (b) the VCD=200 DU).

Also the possibility to apply box AMFs, calculated at different single wavelengths, for the inversion of the BrO SCDs to vertical profiles is discussed. Figure 13 shows the

AMTD
2, 2919–2982, 2009

relative differences between the retrieved BrO profiles and the true profile as function of the wavelength used for the calculation of the box AMFs.

For standard DOAS (case a in Table 7 and upper panel in Figs. 12 and 13) a constant BrO SCD per TH is retrieved for the whole fit window. The variation with wavelength in the difference plot (Fig. 12, upper panel) arises because the true SCDs are wavelength dependent. It can be seen that the discrepancy between the retrieved and the simulated BrO SCD increases for THs where the absorption by ozone is larger (i.e. close to the altitude of the ozone profile peak, compare Fig. 2). Also, this discrepancy depends on the total ozone column: For the case with the ozone VCD=460 DU, the discrepancy is 20% at 19 km and 340.25 nm, and for the case with ozone VCD=200 DU, it is 8%.

Box AMFs should be calculated at a wavelength where the retrieved SCD matches with the true SCD. However due to the strong variation with absorption of ozone and TH it is impossible to select one particular wavelength with the best match that is valid for all ozone profiles (not known a-priori) and THs. This can be seen in Fig. 13, top panel where, for the scenario with the ozone VCD of 200 DU, the best agreement is at 345 nm. At the same time for the scenario with ozone VCD=460 DU this wavelength gives a disagreement of up to 15%.

For the Taylor series approach accounting for the variation of the ozone SCDs in the fit window (case b in Table 7) the fit improves significantly. The fit residual is reduced and it is found that the retrieved BrO SCD (fitted as wavelength independent like in standard DOAS) agrees better with the true wavelength dependent SCDs, in particular at wavelengths where the strongest variation of its absorption cross-section occurs (see second panel from top in Fig. 12). For both scenarios of ozone absorption, the best agreement is found for the wavelength of 344.2 nm. Also further case studies (i.e. with a tropical atmospheric scenario) show a similar agreement (not shown in the figure). Using box AMFs calculated at this wavelength for the profile retrieval, results in a discrepancy between the retrieved and the true profile of less than 3% (see Fig. 13, second panel from top).

AMTD
2, 2919–2982, 2009

For the AMF modified DOAS (case c in Table 7; Figs. 12 and 13) very similar results like for case b can be seen: also here the wavelengths where the fitted BrO SCD agrees with the simulated SCDs are only negligibly changing with TH and ozone profile.

Besides of performing the Taylor series approach for the ozone SCDs, also the description for the optical depth of BrO in the DOAS fit may be improved by including also the first order Taylor series term for the SCD of BrO with respect to wavelength. For case d in Table 7 this term ($S_{\lambda,\mathrm{BrO}}\lambda\sigma_{\mathrm{BrO}}$) is included in the DOAS equation additionally to the Taylor series approach for the ozone SCDs (compare Eq. 18).

Thus the SCDs of BrO are retrieved as a linear function of wavelength. Since the fit is now constrained with two fit arguments for the BrO SCD, a much better agreement between the retrieved and simulated BrO SCDs is achieved (see bottom panel in Fig. 12). The discrepancy is less than 3% not only close to the wavelengths where the more rapid changes in the BrO absorption occur, but also for longer wavelengths (e.g. around 351.5 nm). In comparison to case b, the wavelengths, where the best agreement is found, vary even less with TH and for different ozone profiles, simplifying the selection of an appropriate wavelength for the calculation of the box AMFs. Also, the agreement at longer wavelengths provides an advantage for the calculation of the box AMFs for the inversion, because box AMFs at a longer wavelength have less impact from the absorption of ozone which is generally not known a-priori. Figure 13, bottom panel shows that a good agreement (<3%) between the retrieved and true profile is achieved using box AMFs for inversion of BrO SCDs not only at 344.2 nm, as for the case b, but also around 351.5 nm.

Acknowledgements. We want to thank ESA and DLR for providing the SCIAMACHY level 1 data, and Marcel Dorf for providing the results of the balloon measurements, and Alexei Rozanov for fruitful discussions regarding the BrO profile retrieval, and Andreas Richter for comments on the AMF modified DOAS. One author (S. Kühl) is funded by the DFG (Deutsche Forschungs Gemeinschaft).

The service charges for this open access publication have been covered by the Max Planck Society.

References

Bovensmann, H., Burrows, J. P., Buchwitz, M., Frerick, J., Noël, S., Rozanov, V. V., Chance, K. V., and Goede, A. P. H.: SCIAMACHY: Mission objectives and measurement modes, J. Atmos. Sci., 56, 127–150, 1999. 2945

Brewer, A. W., McElroy, C. T., and Kerr, J. B.: Nitrogen dioxide concentrations in the atmosphere, Nature, 246, 129–133, 1973. 2921

Buchwitz, M., Rozanov, V. V., and Burrows, J. P.: A near-infrared optimized DOAS method for the fast global retrieval of atmospheric CH_4, CO, CO_2, H_2O, and N_2O total column amounts from SCIAMACHY Envisat-1 nadir radiances, J. Geophys. Res., 105(D12), 15231-15245, 2000. 2923

Burrows, J. P., Weber, M., Buchwitz, M., Rozanov, V., Ladstätter-Weißenmayer, A., Richter, A., Debeek, R., Hoogen, R., Bramstedt, K., Eichmann, K.-U., Eisinger, M., and Perner, D.: The Global Ozone Monitoring Experiment (GOME): Mission Concept and First Scientific Results, J. Atmos. Sci., 56, 151–171, 1999. 2921

Butz, A., Bösch, H., Camy-Peyret, C., Chipperfield, M., Dorf, M., Dufour, G., Grunow, K., Jeseck, P., Kühl, S., Payan, S., Pepin, I., Pukite, J., Rozanov, A., von Savigny, C., Sioris, C., Wagner, T., Weidner, F., and Pfeilsticker, K.: Inter-comparison of stratospheric O_3 and NO_2 abundances retrieved from balloon borne direct sun observations and Envisat/SCIAMACHY limb measurements, Atmos. Chem. Phys., 6, 1293–1314, 2006, http://www.atmos-chem-phys.net/6/1293/2006/. 2947

Coldewey-Egbers, M., Weber, M., Buchwitz, M., and Burrows, J. P.: Application of a modified DOAS method for total ozone retrieval from GOME data at high polar latitudes, Adv. Space Res., 34, 749–753, doi:10.1016/j.asr.2003.05.051, 2004. 2923

Coldewey-Egbers, M., Weber, M., Lamsal, L. N., de Beek, R., Buchwitz, M., and Burrows, J. P.: Total ozone retrieval from GOME UV spectral data using the weighting function DOAS approach, Atmos. Chem. Phys., 5, 1015–1025, 2005, http://www.atmos-chem-phys.net/5/1015/2005/. 2923

Deutschmann, T.: Atmospheric radiative transfer modelling using Monte Carlo methods, Diploma Thesis, Universität Heidelberg, 2009. 2931, 2946, 2961

Diebel, D., de Beek, R., Burrows, J. P., Kerridge, B., Munro, R., Platt, U., Marquard, L., and Muirhead, K.: Trace gas study: Detailed analysis of the retrieval algorithms selected for the level 1–2 processing of GOME data, Tech. Rep., Eur. Space Agency (ESA), Section 5,

AMTD
2, 2919–2982, 2009

5–150 pp., 1995. 2922, 2926, 2928, 2935

Dorf, M., Bösch, H., Butz, A., Camy-Peyret, C., Chipperfield, M. P., Engel, A., Goutail, F., Grunow, K., Hendrick, F., Hrechanyy, S., Naujokat, B., Pommereau, J.-P., Van Roozendael, M., Sioris, C., Stroh, F., Weidner, F., and Pfeilsticker, K.: Balloon-borne stratospheric BrO measurements: comparison with Envisat/SCIAMACHY BrO limb profiles, Atmos. Chem. Phys., 6, 2483–2501, 2006, http://www.atmos-chem-phys.net/6/2483/2006/. 2924, 2945, 2947

Dorf, M., Butz, A., Camy-Peyret, C., Chipperfield, M. P., Kritten, L., and Pfeilsticker, K.: Bromine in the tropical troposphere and stratosphere as derived from balloon-borne BrO observations, Atmos. Chem. Phys., 8, 7265–7271, 2008, http://www.atmos-chem-phys.net/8/7265/2008/. 2945, 2947

Fleischmann, O. C., Hartmann, M., Burrows, J. P., and Orphal, J.: New ultraviolet absorption cross-sections of BrO at atmospheric temperatures measured by time-windowing Fourier transform spectroscopy, J. Photoch. Photobio. A, 168, 117-132, 2004. 2948, 2976

Frankenberg, C., Platt, U., and Wagner, T.: Iterative maximum a posteriori (IMAP)-DOAS for retrieval of strongly absorbing trace gases: Model studies for CH_4 and CO_2 retrieval from near infrared spectra of SCIAMACHY onboard ENVISAT, Atmos. Chem. Phys., 5, 9–22, 2005, http://www.atmos-chem-phys.net/5/9/2005/. 2923

Kühl, S.: Quantifying Stratospheric chlorine chemistry by the satellite spectrometers GOME and SCIAMACHY, PhD Thesis, Universität Heidelberg, Heidelberg, Germany, available at: http://www.ub.uni-heidelberg.de/archiv/5664/, 177 pp.,2005. 2946

Kühl, S., Puķīte, J., Deutschmann, T., Platt, U., and Wagner, T.: SCIAMACHY Limb Measurements of NO_2, BrO and OClO, Retrieval of vertical profiles: Algorithm, first results, sensitivity and comparison studies, Adv. Space Res., 42, 1747–1764, 2008. 2924, 2933, 2938, 2946

Marquard, L. C., Wagner, T., and Platt, U.: Improved Air Mass Factor Concepts for Scattered Radiation Differential Optical Absorption Spectroscopy of Atmospheric Species, J. Geophys. Res., 105, 1315–1327, 2000. 2922, 2926, 2927, 2936, 2939

Mount, G. H., Sanders, R. W., Schemltekopf, A. L., and Solomon, S.: Visible spectroscopy at McMurdo Station, Antarctica, 1. Overview and daily variations of NO_2 and O_3, austral spring, 1986, J. Geophys. Res., 92, 8320–8328, 1987. 2921

Noxon, J. F.: Nitrogen dioxide in the stratosphere and troposphere measured by ground-based absorption spectroscopy, Science, 189, 547–549, 1975. 2921

Perliski, L. M. and Solomon, S.: On the evaluation of air mass factors for atmospheric near ultra-violet and visible absorption spectroscopy, J. Geophys. Res., 98, 10363–10374, 1993. 2922

Perner, D., Ehhalt, D. H., Pätz, H. W., Platt, U., Röth, E. P., and Volz, A.: OH-radicals in the lower troposphere, Geophys. Res. Lett. 3, 466–468, 1976. 2921

Pfeilsticker, K. and Platt, U.: Airborne measurements during the Arctic stratospheric experiment: Observation of O_3 and NO_2, Geophys. Res. Lett., 21, 1375–1378, 1994. 2921

Platt, U., Marquard, L., Wagner, T., and Perner, D.: Corrections for zenith scattered light DOAS, Geophys. Res. Lett., 24, 1759–1762, 1997. 2922, 2926

Platt, U., Perner, D., and Pätz, H.: Simultaneous measurement of atmospheric CH_2O, O_3, and NO_2 by differential optical absorption, J. Geophys. Res., 84, 6329–6335, 1979. 2921

Platt, U. and Perner, D.: Direct measurements of atmospheric HCHO, HONO, O_3, NO_2, and SO_2 by differential optical absorption in the near UV, J. Geophys. Res., 85, 7453–7458, 1980. 2921

Platt, U. and Perner, D.: Measurements of atmospheric trace gases by long path differential UV/visible absorption spectroscopy, in: Optical and Laser Remote Sensing, edited by: Killinger, D. K. and Mooradien, A., Springer Series in Optical Sciences, Springer, Berlin, 39, 97–105, 1983. 2921

Platt, U.: Differential Optical Absorption Spectroscopy (DOAS), in: Air Monitoring by Spectroscopic Techniques, edited by: Sigrist, M. W., Chemical Analysis Series, John Wiley, New York, 127, 1994. 2921, 2924, 2925

Platt, U. and Stutz, J.: Differential Optical Absorption Spectroscopy. Principles and Applications, Series: Physics of Earth and Space Environments, Springer, Heidelberg, 597 pp., doi:10.1007/978-3-540-75776-4, 2008. 2921, 2924

Puķīte, J., Kühl, S., Deutschmann, T., Wilms-Grabe, W., Friedeburg, C., Platt, U., and Wagner, T.: Retrieval of stratospheric trace gases from SCIAMACHY limb measurements, Proceedings of the First Atmospheric Science Conference, 8–12 May, ESA/ESRIN, Frascati, Italy, ESA SP-628, available at: http://earth.esa.int/workshops/atmos2006/participants/1148/paper_proc_Frasc_2.pdf, 2006. 2924, 2938, 2946

Richter, A.: Absorptionsspektroskopische Messungen stratosphärischer Spurengase über Bremen, 55° N, Ph.D. thesis, Inst. für Umweltphysik, Univ. of Bremen, Bremen, Germany, 1997. 2922, 2926, 2928, 2935

Rodgers, C. D.: Inverse methods for atmospheric sounding, Theory and practice, World

Scientific Publishing Co. Ltd., Singapore, 2000. 2938, 2947
Rozanov, A., Bovensmann, H., Bracher, A., Hrechanyy, S., Rozanov, V., Sinnhuber, M., Stroh, F., and Burrows, J. P.: NO_2 and BrO vertical profile retrieval from SCIAMACHY limb measurements: Sensitivity studies, Adv. Space Res., 36(5), 846–854, doi:10.1016/j.asr.2005.03.013, 2005. 2950
Solomon, S., Schmeltekopf, A. L., and Sanders, R. W.: On the interpretation of zenith sky absorption measurements, J. Geophys. Res., 92, 8311–8319, 1987. 2921, 2922, 2926
Stutz, J. and Platt, U.: Numerical analysis and error estimation of differential optical absorption spectroscopy measurements with least squares methods, Appl. Optics, 35, 6041–6053, 1996. 2924
Wahner, A., Ravishankara, A., Sander, S., and Friedl, R.: Absorption cross section of BrO between 312 and 385 nm at 298 and 223 K, Chem. Phys. Lett., 152, 507-512, 1988. 2948
Wahner, A., Callies, J., Dorn, H.-P., Platt, U., and Schiller, C.: Near UV atmospheric absorption measurements of column abundances during airborne Arctic stratospheric expedition, January–February 1989: 1. Technique and NO_2 observations, Geophys. Res. Lett., 17, 497-500, 1990. 2921
Wagner, T., Beirle, S., Deutschmann, T., Eigemeier, E., Frankenberg, C., Grzegorski, M., Liu, C., Marbach, T., Platt, U., and Penning de Vries, M.: Monitoring of atmospheric trace gases, clouds, aerosols and surface properties from UV/vis/NIR satellite instruments, J. Opt.-A: Pure Appl. Opt., 10, 104019, doi:10.1088/1464-4258/10/10/1040192008, 2008. 2921
Wilmouth, D. M., Hanisco, T. F., Donahue, N. M., and Anderson, J. G.: Fourier Transform Ultraviolet Spectroscopy of the $A^2\Pi_{3/2} \leftarrow X^2\Pi_{3/2}$ Transition of BrO, J. Phys. Chem. A, 103, 8935–8945, doi:10.1021/jp991651o, 1999. 2948

Table 1. Parameters used for the simulation studies.

Parameter	Description of main settings	Settings for the AMFs comparison	Settings for the sensitivity studies
RTM model	Full spherical 3D Monte Carlo RTM McArtim (Deutschmann, 2009). Simulations for 10 million photon trajectory ensembles. Atmosphere discretized in 1 km layers up to 100 km.		
Atmosphere	Rayleigh atmosphere (i.e. without clouds and aerosols).		
Ground albedo	0.3		
Atmospheric profiles of T, p and trace gases (O_3, NO_2 and BrO). (Profiles of ozone are provided in Fig. 2)	Subarctic scenario corresponding to Kiruna (67.9° N) in March, ozone VCD of 460 DU.	Ozone profile also scaled to 200 DU (additionally to the main setting).	Ozone profile also scaled to 200 DU (additionally to the main setting). Additionally, tropical scenario, (ozone VCD= 270 DU, maximum concentration of ozone at 28 km).
Geometry	Geometry (SZA, SAA) from SCIAMACHY orbit 5545 with SZA at tangent point of 75°, SAA=60°.	Additionally: – AMFs at SZAs of 90°, 88.5° and 43° for nadir. For limb geometry: – AMFs at SZAs=88.5° – AMF for tropical scenario with SZA=43° at tangent point (TP). (For the case with SZA=43°, also ozone profile of 200 DU is applied)	Additionally to the main settings, scenarios with SZA=43° at TP.
Wavelength region	338–357 nm.	AMFs are studied in 332–357 nm region.	Different fit windows within the 332–357 nm region.

AMTD
2, 2919–2982, 2009

Table 2. Variation of AMFs of ozone in the wavelength range of 332–357 nm for different observation geometries and ozone profile with TC of 460 DU (in brackets values for the scenario with TC of ozone of 200 DU are given). The first number gives the difference between maximum and minimum values of AMFs normalized by the mean of AMFs in the wavelength range; the second number is the standard deviation. Calculations are performed only for selected geometries and SZAs in order to illustrate the general tendencies.

SZA (°)	90	88.5	75	43
nadir	24%/6.0%	18%/4.5%	3.1%/0.69%	1.2%/0.26% (1.2%/0.32%)
Limb, TH=19.8 km		20%/4.8%	25%/6.3% (18%/4.8%)	25%/6.1% (18%/4.6%)
Limb, TH=22.8 km			18%/4.3% (12%/3.1%)	
Limb, TH=35.9 km			9.5%/2.0% (4.9%/1.0%)	

AMTD
2, 2919–2982, 2009

Table 3. Relation of the spectral quantities with Eq. (5) and to each other.

	Slant column density	Air mass factor	Optical depth
Relation with SCD	$S(\lambda)$	$\frac{S(\lambda)}{V}$	$S(\lambda)\cdot\sigma(\lambda)$
Relation with AMF	$A(\lambda)\cdot V$	$A(\lambda)$	$A(\lambda)\cdot V\cdot\sigma(\lambda)$
Relation with optical depth	$\frac{\tau(\lambda)}{\sigma}$	$\frac{\tau(\lambda)}{V\cdot\sigma(\lambda)}$	τ
Relation with VCD	$V\cdot A(\lambda)$	$\frac{S(\lambda)}{V}$	$V\cdot A(\lambda)\cdot\sigma(\lambda)$
Relation with vertical optical depth	$\frac{\upsilon(\lambda)\cdot A(\lambda)}{\sigma(\lambda)}$	$\frac{\upsilon(\lambda)}{\sigma(\lambda)}$	$\upsilon(\lambda)\cdot A(\lambda)$
Relation with intensity	$\frac{\ln\frac{I_0}{I}}{\sigma(\lambda)}$	$\frac{\ln\frac{I_0}{I}}{\sigma(\lambda)\cdot V}$	$\ln\frac{I_0}{I}$
	($I(\lambda)$ – intensity, I_0 – intensity without the absorber of interest)		
Relation with Taylor series expansion in Eq. (5)	$F(\lambda)$	$F(\lambda)$	$F(\lambda)\cdot\sigma(\lambda)$

AMTD
2, 2919–2982, 2009

Table 4. Terms of Taylor series expansion considered in the AMF fit study.

	Taylor series terms considered in the fit		
Cases	Constant term	Linear terms	Square terms
Case a	A_0	$A_{\lambda\lambda}$, $A_{O_3}\sigma_{O_3}$	—
Case b	A_0	$A_{\lambda\lambda}$, $A_{O_3}\sigma_{O_3}$, $A_{BrO}\sigma_{BrO}$	—
Case c	A_0	$A_{\lambda\lambda}$, $A_{O_3}\sigma_{O_3}$, $A_{BrO}\sigma_{BrO}$, $A_{NO_2}\sigma_{NO_2}$	—
Case d	A_0	$A_{\lambda\lambda}$, $A_{O_3}\sigma_{O_3}$, $A_{BrO}\sigma_{BrO}$, $A_{NO_2}\sigma_{NO_2}$	$A_{\lambda\lambda}\lambda^2$, $A_{\lambda_{O_3}}\lambda\sigma_{O_3}$, $A_{O_{3O_3}}\sigma^2_{O_3}$

AMTD
2, 2919–2982, 2009

Table 5. Fit terms describing the trace gas absorptions for different approaches in the DOAS fit.

	trace gas		
method	Ozone	BrO	NO_2
Standard DOAS	$S_{O_3}\sigma_{O_3}$	$S_{BrO}\sigma_{BrO}$	$S_{NO_2}\sigma_{NO_2}$
Taylor series approach for ozone SCD	$S_{0,O_3}\sigma_{O_3}$; $S_{\lambda,O_3}\lambda\sigma_{O_3}$; $S_{O_3,O_3}\sigma^2_{O_3}$	$S_{BrO}\sigma_{BrO}$	$S_{NO_2}\sigma_{NO_2}$
AMF modified DOAS for ozone	$V_{O_3}A_{O_3}\sigma_{O_3}$	$S_{BrO}\sigma_{BrO}$	$S_{NO_2}\sigma_{NO_2}$

AMTD
2, 2919–2982, 2009

Table 6. Characterization of the BrO retrieval results obtained by different methods and applying different fit windows. Text in bold indicates overall good agreement, text in italic significant disagreement.

Fit window	Nr. of BrO absorption bands	Standard DOAS	Taylor series approach	Taylor series approach, correction for broadband wavelength dependency by wavelength term ($S_{\lambda,O_3}\lambda\sigma_{O_3}$) only	Taylor series approach, correction for ozone absorption structures by ozone absorption term ($S_{O_3,O_3}\sigma^2_{O_3}$) only
(1)	(2)	(3)	(4)	(5)	(6)
332–357 nm	5	*Underestimation of profile (by 40% at the peak, up to 100% above the peak)*	**Good agreement**	*Underestimation of profile (by 20% at the peak)*	*Overestimation of profile above the peak by ~5–10%, similar underestimation below the peak*
332–351.1 nm	4	*Similar as above*	**Good agreement**	*Underest. (by 15–20% at the peak)*	*Similar as above*
332–346.6 nm	3	*Shape of profile similar as above, underestimation increases*	**Slightly underestimated values below the peak (bellow 5%)**	*Similar as above*	Good agreement at and above the peak, however some absorption structures of ozone unfitted

AMTD
2, 2919–2982, 2009

Table 6. Continued.

(1)	(2)	(3)	(4)	(5)	(6)
332–339.9 nm	2	*Shape of profile similar as above, underestimation strongly increases (discrepancy more than 60% at the peak, large negative values at 18–28 km)*	*Underestimation of profile above the peak by ~10% and very prominent overestimation below the peak by ~30%*	*Overestimation of profile above the peak by ~5% and underestimation at the peak and below by ~20%*	*Prominent underestimation of profile above the peak by 30–40%*
338–357 nm	4	*Overestimated above the peak and at the peak (by ~10% at the peak and even more above the peak) and overestimated below the peak (profile shifted upwards)*	**Good agreement above the peak, underestimation (~5%) at peak, overestimation (up to 10%) below the peak**	Good agreement in range of ~5% at the peak (some small unfitted absorption structures of ozone present that potentially may affect the retrieval)	Good agreement in range of ~5% at the peak (relatively strong unfitted absorption structures of ozone present that potentially may affect the retrieval)
338–351.1 nm	3	*Shape of profile similar as above (profile shift upwards). Even more overestimated above the peak and at the peak (~20%) and overestimated below the peak*	**similar as above**	similar as above	*Overestimation of profile at the peak ~10%*

Table 6. Continued.

(1)	(2)	(3)	(4)	(5)	(6)
338–346.6 nm	2	*The distortion of profile even more pronounced as for the two examples above, overestimated by more than ~30%*	similar as above, although the at the peak the discrepancy is few percent larger	Disagreement for most of the parts of profile by ~5%	*Overestimation of profile at the peak larger as above in the range of 15%.*
341.3–357 nm	3	*Underestimation by 30% at the peak and above the peak and increase by 30% at 12 km (Profile shift downwards)*	**Overall good agreement except underestimation at the peak by ~5%**	**Overall good agreement except underestimation at the peak by ~5%**	*Underestimation at the peak and above by ~10%, overestimation below the peak by ~5%*
341.3–351.1 nm	2	*Shape similar as above, although systematial error is by ~10% smaller*	**Overall good agreement**	**Overall good agreement**	*Underestimation at the peak and above by ~15%, overestimation below the peak by ~5–10%*
347.8–357 nm	2	**Overall good agreement**	**Overall good agreement**	**Overall good agreement**	**Overall good agreement**

AMTD
2, 2919–2982, 2009

Table 7. Fit terms describing the trace gas absorptions for different approaches in the DOAS fit and equations for the estimation of the BrO SCD from the fitted coefficients.

Cases, short description	Ozone	NO_2	BrO	Estimation for the SCD of BrO
Case a (Standard DOAS)	$S_{O_3}\sigma_{O_3}$	$S_{NO_2}\sigma_{NO_2}$	$S_{BrO}\sigma_{BrO}$	S_{BrO}
Case b (Taylor series approach only for ozone SCD)	$S_{0,O_3}\sigma_{O_3}$; $S_{\lambda,O_3}\lambda\sigma_{O_3}$; $S_{O_3,O_3}\sigma^2_{O_3}$	$S_{NO_2}\sigma_{NO_2}$	$S_{BrO}\sigma_{BrO}$	S_{BrO}
Case c (AMF modified DOAS for ozone SCD)	$V_{O_3}A_{O_3}\sigma_{O_3}$	$S_{NO_2}\sigma_{NO_2}$	$S_{BrO}\sigma_{BrO}$	S_{BrO}
Case d (additionally the broad band variation with wavelength on the BrO SCD is considered)	$S_{0,O_3}\sigma_{O_3}$; $S_{\lambda,O_3}\lambda\sigma_{O_3}$; $S_{O_3,O_3}\sigma^2_{O_3}$	$S_{NO_2}\sigma_{NO_2}$	$S_{0,BrO}\sigma_{BrO}$; $S_{\lambda,BrO}\lambda\sigma_{BrO}$	$S_{0,BrO}+S_{\lambda,BrO}\lambda$

AMTD
2, 2919–2982, 2009

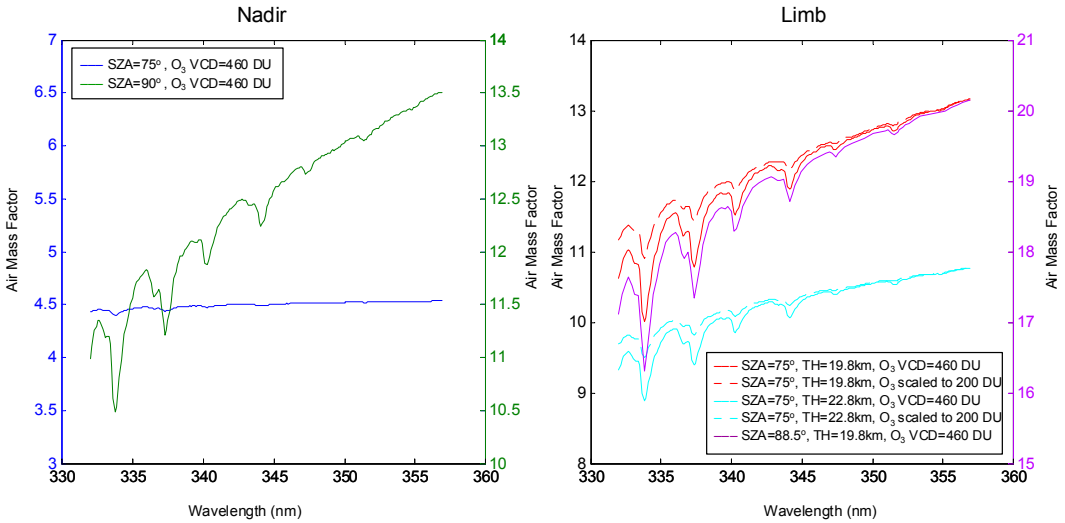

Fig. 1. AMFs of ozone for nadir (left) and limb geometry (right) as function of wavelength for different atmospheric scenarios (see legend and Table 1 for details).

AMTD
2, 2919–2982, 2009

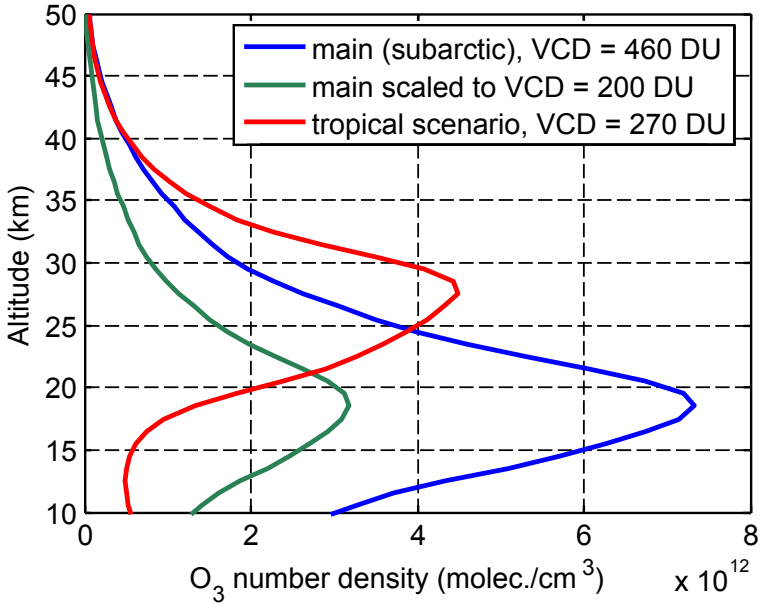

Fig. 2. Different ozone profiles applied for the spectra simulations, air mass factor calculations and sensitivity studies.

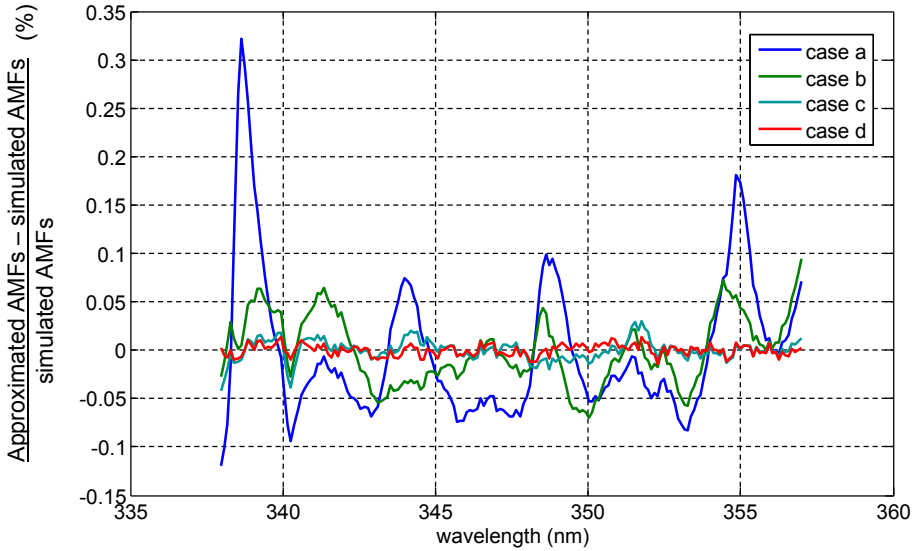

Fig. 3. Relative difference between AMFs of ozone approximated by Taylor series and simulated AMFs for the main settings (see Table 1). The different lines correspond to the results obtained by considering different number of Taylor series terms as fit parameters as listed in Table 4. The difference is averaged for all tangent heights. Compare with Fig. 1 to see the improvement with respect to a constant AMF.

AMTD
2, 2919–2982, 2009

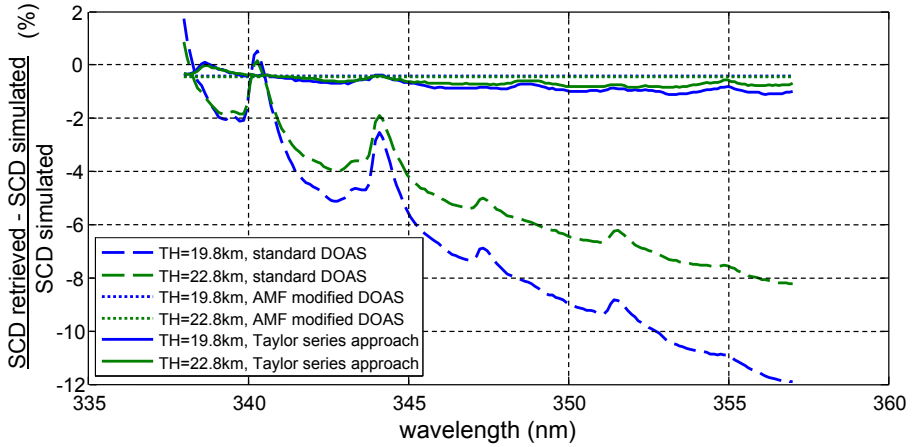

Fig. 4. Relative difference between the retrieved and the true (simulated) ozone SCDs using different approaches. Plots are for two THs near the peak of the ozone profile (19.8 and 22.8 km). The same relative differences are valid also for the relation between fitted and true optical depths.

AMTD
2, 2919–2982, 2009

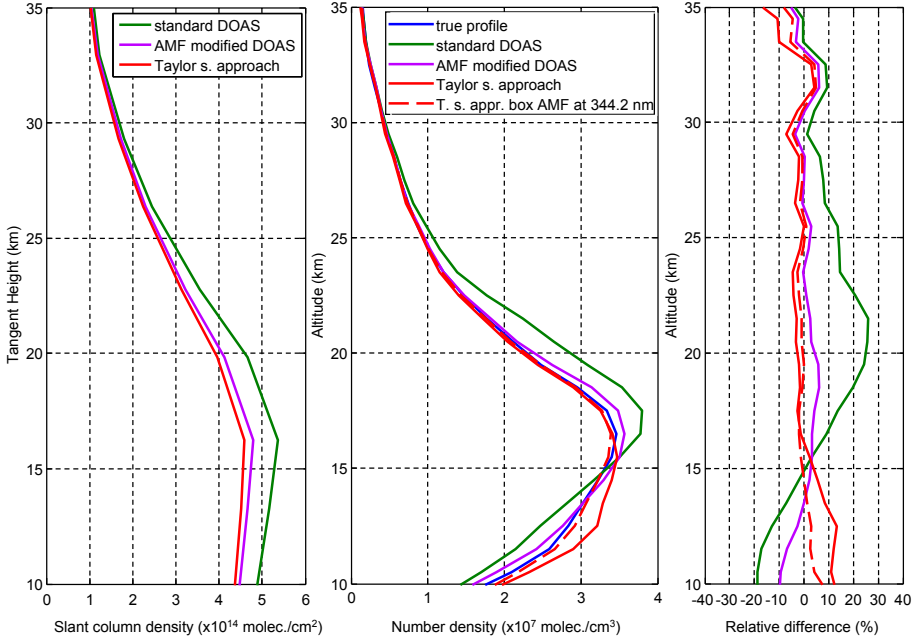

Fig. 5. BrO SCDs (left panel) and the vertical concentration profiles (middle panel) retrieved by different approaches (green: standard DOAS, violet: AMF modified DOAS, red: Taylor series approach, dashed red: AMFs for the Taylor series approach evaluated at a single wavelength of 344.2 nm). The right panel shows the relative difference of the retrieved profiles to the true concentration profile applied for the simulation.

AMTD
2, 2919–2982, 2009

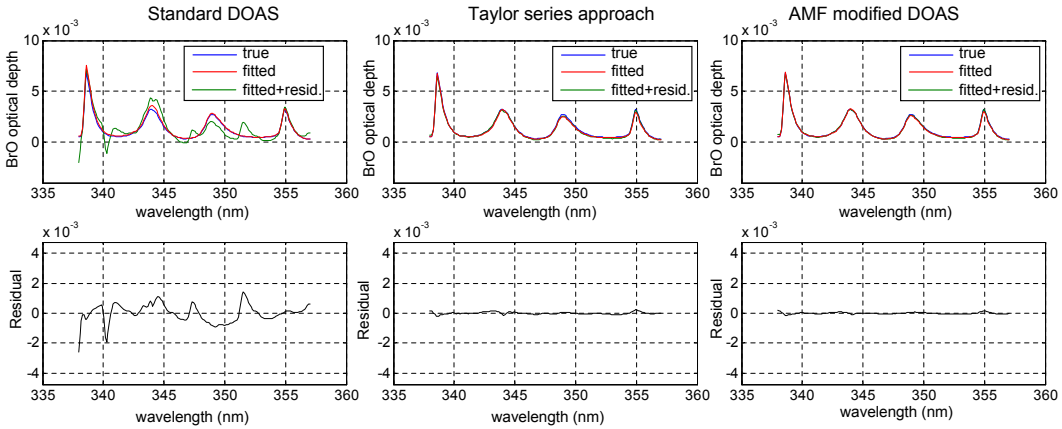

Fig. 6. Left panel: Retrieved optical depth of BrO for TH=22.8 km by the standard DOAS fit. Middle panel: same but for the Taylor series approach. Right panel: same but for AMF modified DOAS for ozone. Top panels show the true optical depth of BrO (blue), fitted optical depth of BrO (red) and the optical depth plus residual structures (green). The bottom panels show the residuals alone.

AMTD
2, 2919–2982, 2009

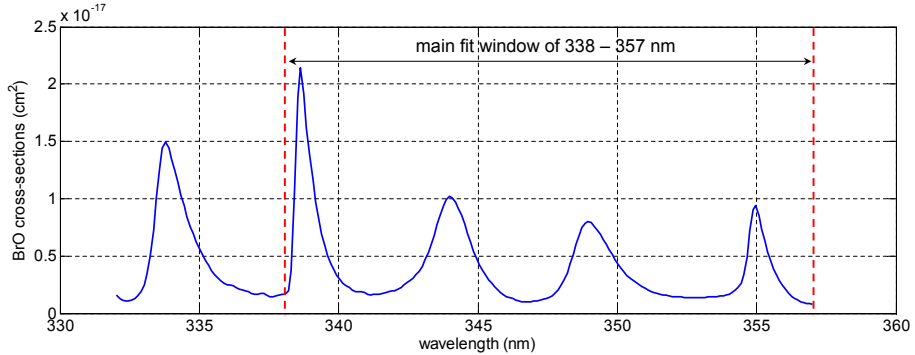

Fig. 7. BrO absorption cross-section used for spectra simulations (Fleischmann et al. (2004), convolved to SCIAMACHY resolution of FWHM of 0.21 nm). In the main settings the fit window from 338-357 nm is applied (indicated in the plot by red lines). For the sensitivity studies, different fit windows containing 2–5 BrO absorption peaks within the wavelength region from 332–357 nm are investigated.

AMTD
2, 2919–2982, 2009

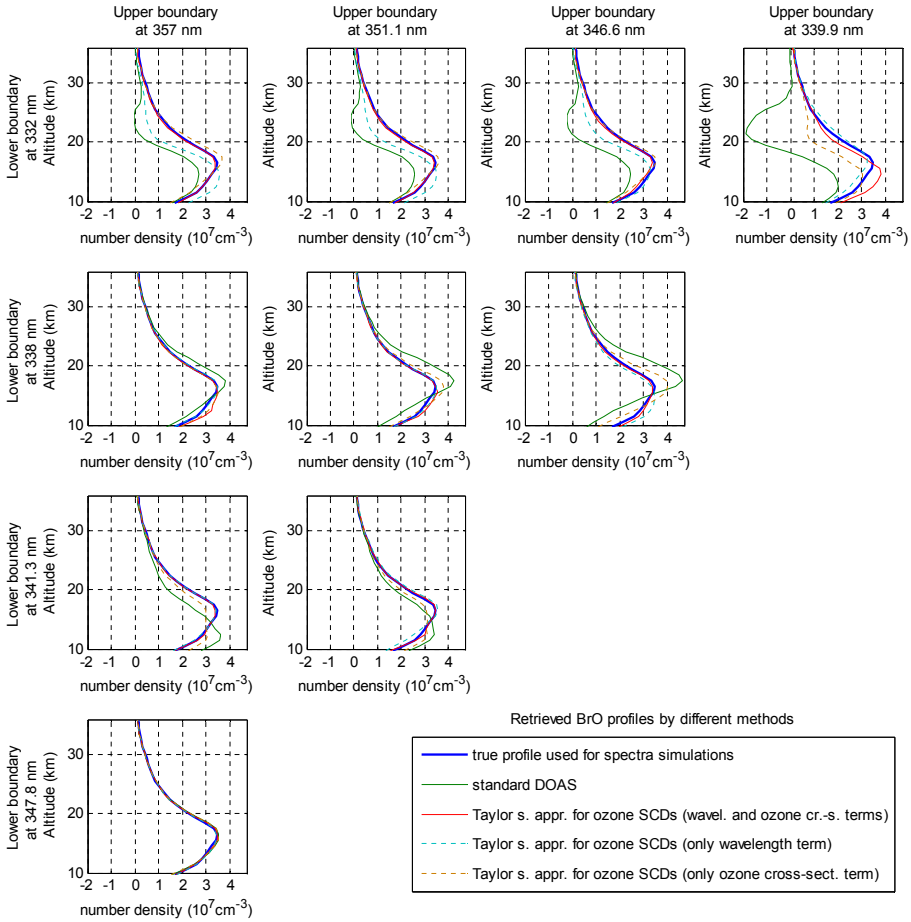

Fig. 8. Vertical profiles of the BrO number density retrieved from the simulated spectra for different fit windows and different retrieval approaches. Plots in the same row correspond to the same lower boundary of the fit window, plots in the same column, to the same upper boundary of the fit window.

AMTD
2, 2919–2982, 2009

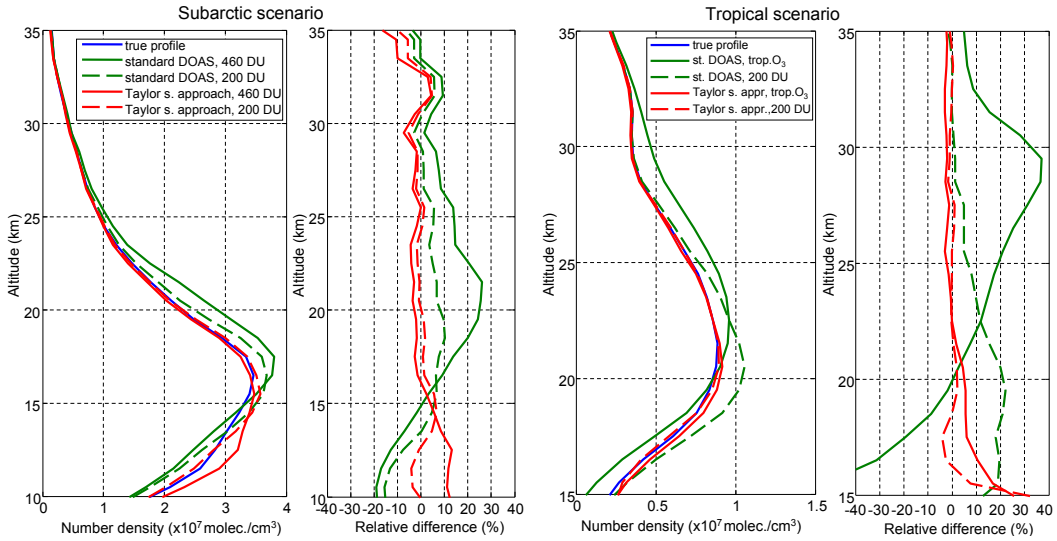

Fig. 9. Retrieved concentration profiles of BrO from simulated spectra by the standard DOAS and Taylor series approach (odd panels from left) and the relative differences with the true profile (even panels from left). First two panels on left: the result for the subarctic atmospheric scenario where besides the simulation of spectra using ozone profile with VCD=460 DU also simulation for an ozone profile scaled to TC=200 DU is performed. First two panels on right: the result for the tropical scenario, not only with tropical ozone profile with maximum at 28 km but also for a subarctic profile (scaled to 200 DU) with peak at 19 km.

AMTD
2, 2919–2982, 2009

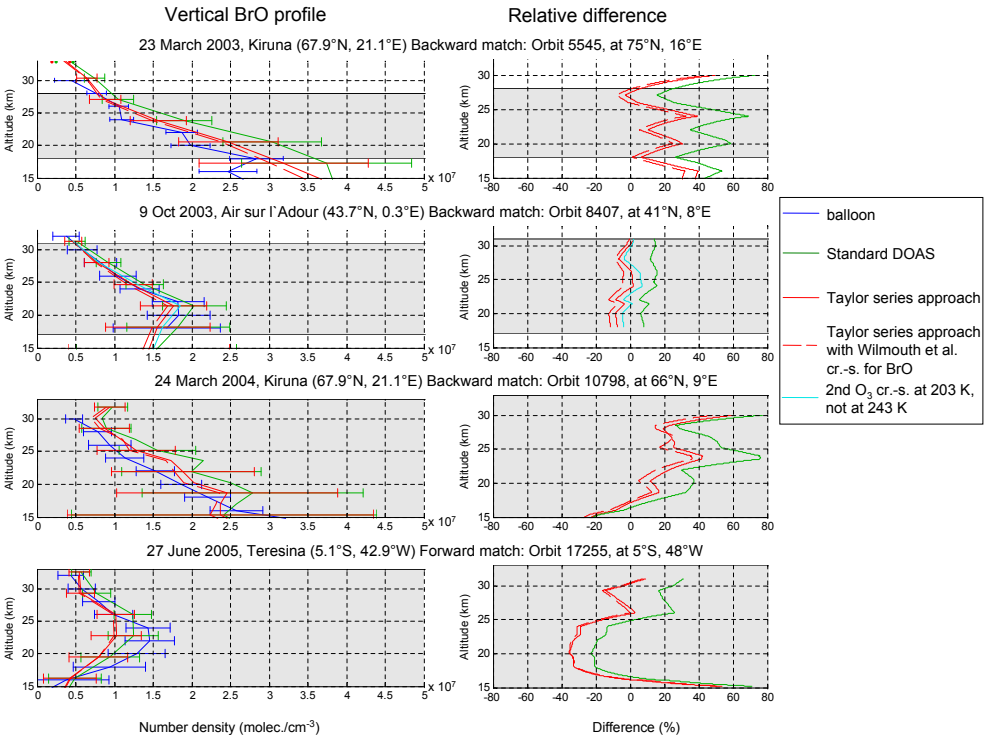

Fig. 10. Comparison of BrO profiles derived from balloon observations (Dorf et al., 2006, 2008) with SCIAMACHY limb retrievals for four different balloon launches as indicated on the titles of the panels. Shown is the comparison either for the backward or the forward match of the trajectory modelling. Always the match with the largest altitude range with correlated data is chosen. The altitude range where the sounded air masses match is indicated as a grey area. On the left panel the blue lines represent the balloon profiles photochemically corrected to match the SZA of the SCIAMACHY measurement (except the Teresina launch where the original profile is plotted). The SCIAMACHY measurements are shown as red lines for the Taylor series approach and as green lines for the standard DOAS. Retrieval with BrO cross-sections of Wilmouth et al. (1999) is shown as dashed lines. For the measurements at Aire sur l'Adour, also retrieval with the additional ozone cross-sections at 203 K (replacing the cross-sections at 243 K) is included in the plot (cyan line). On the right panel the relative differences between the SCIAMACHY and balloon profiles are shown.

AMTD
2, 2919–2982, 2009

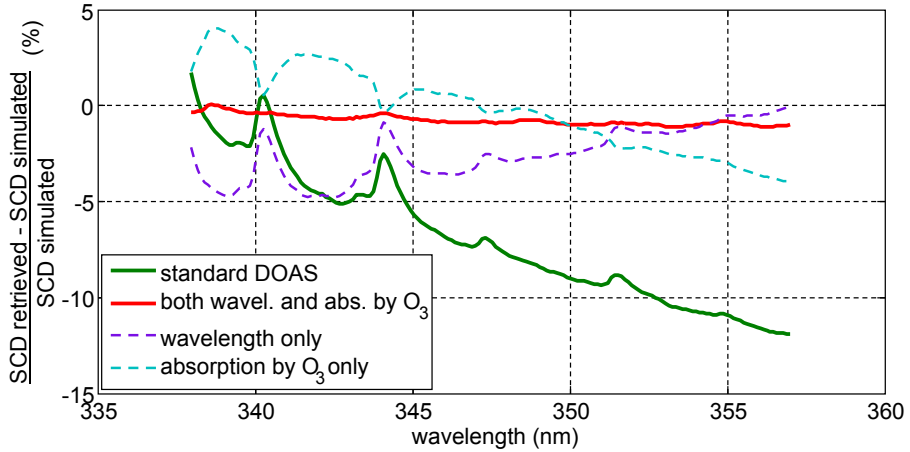

Fig. 11. Relative difference between the retrieved SCDs and the true (simulated) SCDs of ozone at TH=19.8 km if different terms describing the variation of SCD of ozone in the fit window are considered.

AMTD
2, 2919–2982, 2009

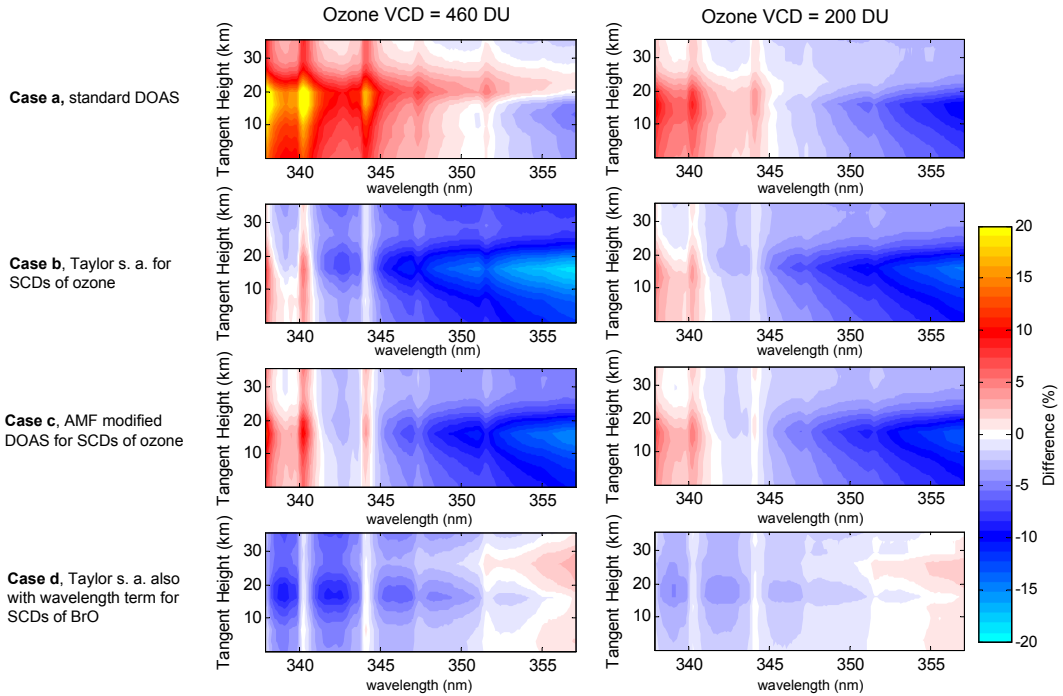

Fig. 12. Relative difference between retrieved SCDs of BrO and the true (simulated) SCDs as function of TH and wavelength for the studied cases (a)–(d) (see Table 7). The retrievals were performed for two different ozone profiles (with VCD=460 DU, on the left, and 200 DU, on the right, see Fig. 2.)

AMTD
2, 2919–2982, 2009

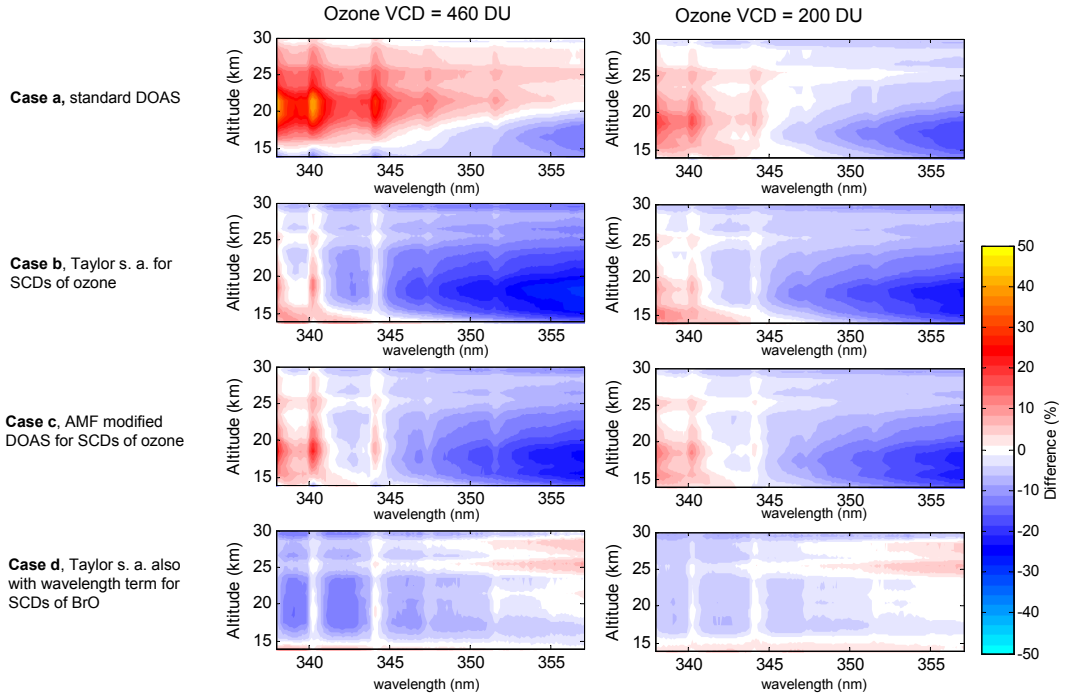

Fig. 13. Same as for Fig. 12 but relative differences between retrieved profiles applying box AMFs calculated at different wavelengths (x-axis) and the true vertical profile of BrO are shown.

AMTD
2, 2919–2982, 2009